Peptide-functionalized hydrogels for three-dimensional cell culture

A Thesis
SUBMITTED TO THE FACULTY OF
UNIVERSITY OF MINNESOTA
BY

Carolyn M. Scott

IN PARTIAL FULFILLMENT OF THE REQUIREMENTS
FOR THE DEGREE OF
DOCTOR OF PHILOSOPHY

Efrosini Kokkoli

June 2016

Acknowledgements

I have truly enjoyed my time at the University of Minnesota thanks to the help, support, and friendship of many wonderful people. I'd like to thank my advisor, Efie, for her guidance and support throughout this project. This work relied on the help and support of the staff at the University Imaging Centers and the Polymer Characterization Facility. Specifically, I'd like to thank John Oja and Guillermo Marques for their patience and help with confocal microscopy. I'd also like to thank David Giles for his expertise and creative solutions related to rheology. I am very grateful to have been supported by the NIH Biotechnology Training Grant, which allowed me to get to know graduate students in other departments and complete a summer internship at Surmodics.

I must also thank the members of the Kokkoli group, past and present, for their help and support. In particular, I want to thank Brett Waybrant, Maroof Adil, Nicole Atchison, Matt Petersen, Tim Pearce, Rachel Levine, Frankie Paleaz and Mike Harris, for creating a supportive and collaborative work environment in the office. I would also like to thank members of the Hackel lab for their help and equipment. I especially thank Sadie Johnson and Larry Stern for their willingness to serve as a science sounding board and their help trouble shooting experiments and asking the right questions. Finally, I'd like to thank my family for their love and support throughout the stress and struggles of grad school.

Abstract

Biomimetic scaffolds have played a major role in the advancements in tissue engineering. In addition to mimicking the stiffness, nanofibrous structure, and biochemistry of the native extracellular matrix (ECM), reproducing the three-dimensional (3D) environment of the ECM has been shown to be extremely important. To this end, we designed a co-assembling peptide-amphiphile hydrogel system containing the fibronectin-mimetic PR_g peptide-amphiphile and an E2 diluent peptide-amphiphile for the entrapment and culture of cells in 3D. The E2 diluent peptide amphiphile was designed to screen charges on the PR_g and increase the kinetics of self-assembly in physiologically relevant solutions. Our study investigated two weight percent formulations, 0.5 and 1.0 wt %, and found that in both, entrapped fibroblasts survived encapsulation, proliferated, and deposited collagen IV and fibronectin ECM proteins. The 0.5 wt % gels had a modulus of 429 Pa and supported significantly more fibroblasts proliferation than the 1.0 wt % gels, which had a modulus of 809 Pa. The 1.0 wt% gels though, supported significantly higher mRNA expression and production of ECM proteins. This result indicates by tuning the wt % of our peptide-amphiphile hydrogels, we can encourage either rapid proliferation or ECM deposition.

While peptide-amphiphiles are an attractive material for the design of cell scaffolds due to their ability to self-assemble into nanofibrous hydrogels and incorporate multiple

biomimetic peptides, there are some limitations associated with these physical hydrogels. One such limitation is that the kinetics of assembly and the mechanical properties of the resulting hydrogels are dependent upon the peptide sequence. We found that the modulus of multifunctional peptide-amphiphile hydrogels ranged from 1000 to 6500 Pa, which was too broad a range to deconvolute the effect of the peptide signal and the effect of mechanical properties.

To simplify our system and study the effects of combining ECM protein-mimetic and growth factor-mimetic peptides on the proliferation and function of pancreatic β-cells, peptide mimetics were covalently immobilized on plates. This study found that β-cells proliferate more and secreted significantly more insulin on peptide-functionalized compared to non-functionalized controls. The specific peptide mimetic or combination of peptide mimetics did not significantly affect insulin secretions, but literature suggests that other signals, including cell-cell signaling may play a more significant role in insulin secretion than ECM protein or growth factor signaling. A poly(ethylene glycol) dimethacrylate (PEGDM) hydrogel was functionalized with the laminin-mimetic IKVAV peptide at a 20 μM concentration to match the modulus of non-functionalized hydrogels. This system was used to determine if peptide-functionalization also had an effect in 3D. We found β-cells in IKVAV-functionalized hydrogels proliferated significantly more than β-cells in non-functionalized scaffolds, but no differences in insulin secretion were

observed. Together, these studies demonstrate the ability of peptide mimetics to enhance cell proliferation and function of cells in 2D and 3D culture.

Table of Contents

List of Tables

List of Figures

Chapter 1 Introduction

Since its inception in the early 90's, tissue engineering has promised to be a powerful therapy in modern medicine; an answer to the shortage, cost, and complications associated with organ and tissue transplantation. Tissue engineering requires the appropriate interaction of cells, scaffolds, and biochemical signals such as mitogens and growth factors. The realization of importance of the mechanical, structural, and biochemical properties of the native extracellular matrix (ECM) has led to the development of new techniques and chemistries to form and functionalize scaffolds for cell culture. While many scaffolds are readily modified to mimic the architecture and mechanical properties of native ECM, most scaffolds grossly oversimplify its biochemical complexity. Often a single bioactive ligand or protein is used to mimic ECM function and as a result many scaffolds fail to support cell adhesion, survival and phenotype maintenance long term.[1] Additionally, scaffolds with multiple functional ligands typically do not diversify functional properties of the ECM and include only one class of bioactive ligand rather than combinations of multiple classes of functional molecules. This work focuses on the translation of a fibronectin-mimetic self-assembling peptide-amphilphile hydrogels to 3D for cell entrapment and the incorporation of additional peptide cell binding and growth factor binding domains to be combined in a

modular fashion to produce defined, multicomponent hydrogels, optimized to support the culture and differentiation of different cells.

1.1 The extracellular matrix

The extracellular matrix (ECM) is a collection of fibrous proteins and proteogylcans which provide essential structure support and biochemical and biomechanical cues to cells in tissues and organs. Some of the major protein components include fibronectin, collagens, elastins, and laminin. Proteoglycans consist of a core protein covalently decorated with glycosaminoglyans (GAGs); they are extremely hydrophilic and fill the majority of the ECM. Due to their ability to take up water, proteoglycan rich ECMs are able to withstand high compressive forces. Both proteins and proteoglycans have the ability to bind growth factors.[2] Each tissue ECM has a unique composition and architecture which is optimized for that tissue's specific function.

1.1.1 Collagen

Collagen is the most abundant fibrous protein in the extracellular matrix which provides tensile strength and supports cell adhesion and migration. Fibroblasts are predominantly responsible for the synthesis of the many different types of collagen, the most common are type I, II, and III. Type I collagen is abundant in skin, tendon, bone, ligaments, and dentin. Type II collagen is the major collagen in cartilage and type III collagen is found in skin, muscle, tendon and dentin. Type IV collagen is not the most abundant of the

collagens, but it is found in the basil lamina of all tissues. Fibrous collagen is made up of three α-chains to form a triple helix with the NC1 and 7S domains at the N- and C-terminus respectively (Figure 1.1). The triple helix domain is made up of the characteristic repeating unit: Gly-Pro-X, where X can be any amino acid. The collagen triple helices, called collagen fibrils, align and assemble with other fibrils to form bundles of fibrous collagen.

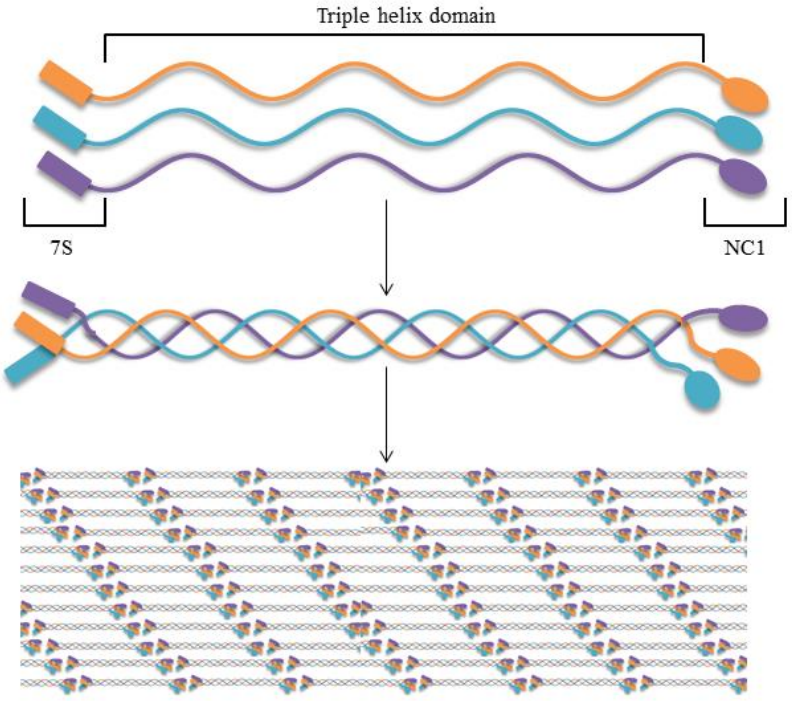

Figure 1.1: Schematic of collagen structure and assembly.

1.1.2 Fibronectin

The ECM protein fibronectin is involved in many cell processes; including cell adhesion, cell migration, and differentiation of stem cells. Fibronectin exists as a dimer, consisting of two similar subunits, which contain binding domains for fibrin, heparin, collagen, and cells. These subunits are crosslinked by disulfide bonds at their C-terminal ends (Figure 1.2). Each subunit is made up of serially-repeating modules named type I, type II, and type III.[3] The ubiquitous RGD cell binding domain is located in the 10^{th} type III repeat of fibronectin and the PHSRN synergy domain located in the 9^{th} type III repeat of fibronectin.[4] The crystal structure of the $III_{7\text{-}10}$ domains of fibronectin reveal that these cell binding and synergy sites are separated by 30-40 Å and extend approximately 10 Å away from the surface of the protein. The RGD sequence has been extensively used to facilitate cell adhesion on biomaterials and it has been shown to bind a variety of integrins, including $\alpha_5\beta_1$, $\alpha_v\beta_3$.[5] During embryonic development fibronectin is very highly expressed, but its expression progressively decreases with age.[6] Despite this decrease in expression during development, fibronectin is found in the basal lamina of most adult tissues.

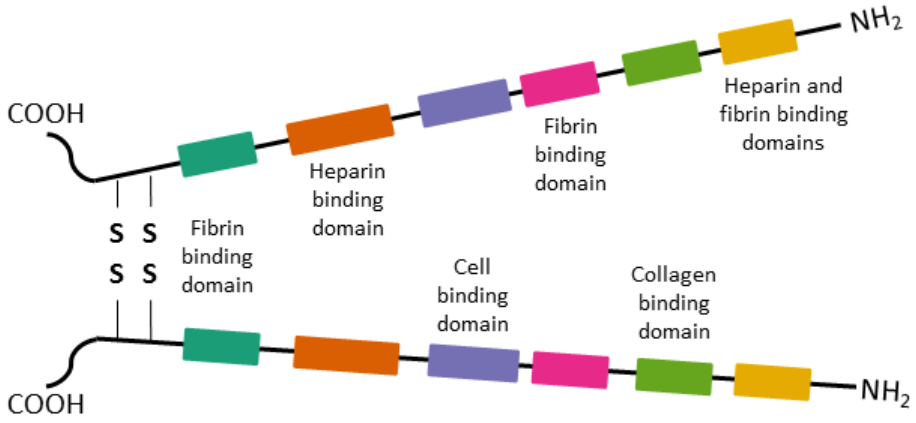

Figure 1.2: Schematic of fibronectin structure and domains.

1.1.3 Laminin

Laminin is the principle matrix protein in the basal lamina. Laminin is a heterotrimeric protein, composed of and α-chain, a β-chain, and a γ-chain. The cross-like structure, shown in Figure 1.3 contains binding domains for collagens, cells and integrins. The three subunits form an α-helical coiled coil and are linked by several disulfide bonds.[2] Laminins bind a several integrins, including $\alpha_3\beta_1$, $\alpha_2\beta_1$, $\alpha_6\beta_1$, and $\alpha_6\beta_4$, and mediates adhesion of a variety of cells, including endothelial cells, epithelial cells, and neurons. Laminin is a major component of neural ECM and has been shown to improve neuron differentiation and axon outgrowth in vitro.[7] The RGD cell binding domain found in fibronectin is also present in laminin. Other cell binding domains in laminin include the YIGSR and IKVAV cell binding domains. The YIGSR and RGD domains have been shown to mediate the attachment and differentiation of endothelial cells.[8]

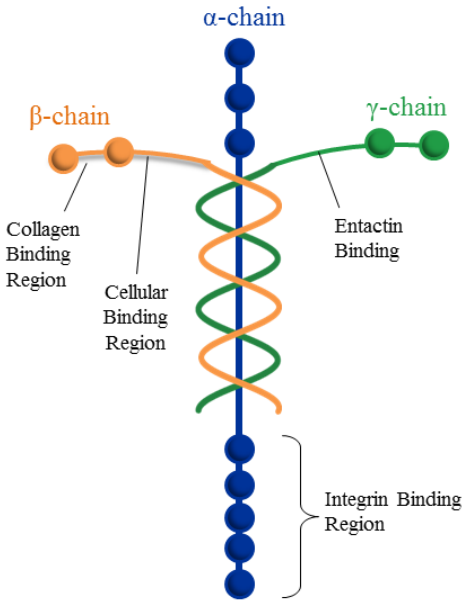

Figure 1.3: Schematic of laminin structure and domain.

1.2 Biomaterials scaffolds for tissue engineering

Tissue engineering scaffolds are designed to mimic the mechanical, biochemical and architectural properties of the extracellular matrix (ECM). Two of the most common classes of materials for scaffolds are synthetic polymers, such as poly(ethylene glycol) (PEG) and poly(lactic-co-glycolic acid) (PLGA) and natural biopolymers, such as collagen, chitosan, and fibrin. While synthetic polymers lack the innate bioactivity found in natural biopolymers, many synthetic scaffolds can be readily modified to mimic the nanofibrous architecture and mechanical properties of native ECM by modifying monomer size, crosslinking, and electrospinning or curing conditions. Natural

biopolymers are innately nanofibrous and bioactive, but they are potentially immunogenic, there can be batch to batch variability, and they are limited to a narrower range of mechanical properties compared to synthetic polymers.

1.3 Biochemical functionalization

With few exceptions, mammalian cells are anchorage dependent, requiring adhesion to a substrate to maintain cell viability.[9] Without the associated tension generated from binding to a substrate, binding of ECM proteins or peptides in solution results in cell death. To encourage cell adhesion to scaffolds, bioactive molecules are incorporated. Bioactive proteins and peptides have been adsorbed to scaffolds or covalently immobilized using a variety of chemistries, including N-hydroxysuccinimide esters (NHS), maleimide, or "click" chemistry. Functionalization of scaffolds with the entire bioactive molecule or with smaller domains and peptides, including the RGD peptide, has been studied. While the use of full proteins can provide the benefits of secondary and tertiary structure, they can be immunogenic. Additionally, protein denaturation or unfolding often occurs during adsorption and can be disrupted by immobilization chemistries. Due to their large size, there is a lack of control over protein presentation and orientation on scaffolds. The small size of peptides provides high stability and control over the presentation of bioactive domains for scaffold functionalization. Peptides have been used to great effect to increase cell adhesion to many materials, including metal and ceramic substrates and synthetic polymer hydrogels.

Most scaffolds fail to successfully reproduce the complex biochemical signaling and functions of the native ECM as they are functionalized with at most two bioactive molecules.[10–13] As a result of this oversimplified functionalization, many scaffolds fail to support long term cell adhesion, survival and phenotype maintenance. Some of the challenges limiting diverse biochemical functionalization of tissue engineering scaffolds include the requirements for control over molecular orientation and mild chemistries to preserve biological activity. Polymeric scaffolds are also constrained by the limited number of unique, compatible chemistries for the addition of bioactive molecules. The interactions of the many components of the ECM and their effect on its complex function are poorly understood. Thus far, no study to our knowledge has investigated whether the benefits of scaffold functionalization with multiple classes of ligands are significant or additive. Different studies have functionalized scaffolds with peptides derived from laminin (IKVAV or YIGSR),[14,15] fibrinogen (KQAGDV),[15] collagen (GTPGPQGIAGQRGVV or TAGSCLRKFSTM),[15,16] or the RGD ligand[17] and have shown that by selecting a functional ligand derived from the cell's native ECM cell adhesion, proliferation, and differentiation efficiency are improved. Thus, the design of modular tissue engineering scaffolds capable of more complex mimicry of the natural ECM would allow for exploration of combinatory approaches to scaffold functionalization which could, in turn, significantly contribute to advances in the fields of cell biology, tissue engineering and regenerative medicine.

1.4 Mechanical properties

Reproducing the mechanical properties of a cells' native environment has been shown to influence cell morphology, migration, gene expression, and function as well as to influence the differentiation of stem cells.[18–21] NIH3T3 fibroblasts have demonstrated preferential migration from soft surfaces to stiff surfaces, and have larger focal adhesions on stiffer substrates, likely as result of increased mechanotransduction.[22] There is evidence that substrate stiffness plays as large a role in stem cell differentiation as biochemical signaling patterns and growth factor treatments.[23–25] Mesenchymal stem cells have been shown to differentiate towards neural, myogenic, or osteogenic fates as a result of substrate stiffness alone.

The elastic modulus of human tissues spans from very soft to very stiff. Neural tissue has an elastic modulus of approximately 0.1 kPA, pancreatic tissue is ~1 kPa, muscle is ~10 kPa and bone is ~100 kPA.[23,26] The modulus of engineered scaffolds should be designed to match the mechanical properties of the native tissue. Mechanical properties of scaffolds can be tuned by adjusting the concentration of chemical crosslinkers; adjusting the molecular weight of the monomer, and thus the length between crosslinks; or adjusting the weight percent of scaffold material forming the hydrogel.[27–30]

1.4.1 Dimension

Three-dimensional culture provides cells with a more realistic mimetic of a natural, in vivo environment compared to traditional two-dimensional culture. Literature suggests 3D cell culture is critically important for tissue engineering applications, as 2D cell culture introduces an artificial polarity between cells' upper and lower surfaces resulting in non-native cell morphologies and expression profiles.[31] Cells have been shown to proliferate and migrate faster in 3D culture[32] and there is evidence that integrin and receptor expression varies between 2D and 3D culture environments.[33,34] Three dimensional culture of hepatocytes has indicated that 3D environments slow the dedifferentiation of hepatocytes and non-parenchymal hepatic cells *in vitro*, increasing the amount of culture time and the expansion potential of hepatocytes with maintained mature function.[35–37] Dermal keratinocytes and fibroblasts have improved viability when exposed to cytotoxic agents when cultured in 3D scaffolds compared to traditional 2D tissue culture plastic.[38] These a just a few examples highlighting the importance of reproducing the dimensionality of a cells' native environment in addition to the biochemical and mechanical properties.

1.5 Peptide-amphiphiles

Amphiphiles are molecules that contain hydrophilic and hydrophobic domains. Peptide amphiphiles (PAs) have a hydrophilic peptide headgroup covalently attached to a

hydrophobic hydrocarbon tail (Figure 1.4). The hydrophobic tail is most often an alkyl or dialkyl hydrocarbon chain with 12-20 carbons,[39] but hydrophobic polymers have also been used.[40] The size of the peptide headgroup is typically 5-20 amino acid residues and is considered to have at least two distinct domains.[41] A spacer sequence, adjacent to the hydrophobic tail is often included to control assembly and increase accessibility of a functional peptide.[42,43] The functional peptide domain is often a bioactive peptide signal or a charged sequence which can provide additional control over peptide-amphiphile assembly.[44] Entropic interactions with the surrounding medium drive the self-assembly of peptide-amphiphiles into various structures, such as micelles, vesicles, bilayers, nanofibers and ribbons.[45] Peptide amphiphiles with single tails and bulky, hydrophilic headgroups have an overall conical shape and tend to form nanofibers.[46] This is a desirable structure because nanofibers have been identified as a key feature of tissue engineering scaffolds, as they mimic the structural architecture of the natural ECM in tissues.[47]

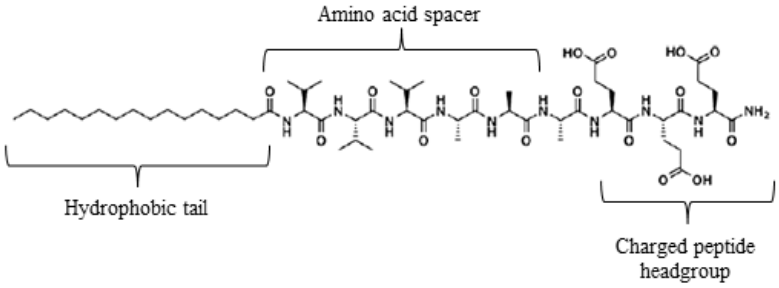

Figure 1.4: Structure of a peptide-amphiphile with a hydrocarbon tail, a peptide spacer, and a charged peptide domain.

In aqueous environments, the hydrophobic tails are arranged in the core of the nanofiber and the hydrophilic peptide domains interact with water. TEM imaging, infrared spectroscopy, and circular dichroism methods have shown that β-sheet secondary structures are a common characteristic of peptide-amphiphiles which form cylindrical micelle nanofibers.[44,48–50] Spectroscopy indicates that β-sheet-like hydrogen bonding occurs between peptide amphiphiles along the length of the nanofiber[50] contributing to nanofiber stability while interactions in the radial direction are primarily electrostatic.[51] The first 5 amino acid residues adjacent to the hydrocarbon tail are critically important for β-sheet and nanofiber formation.[49] Amino acid residues with bulky side chains including valine, isoleucine, phenylalanine, threonine, tryptophan, and tyrosine favor β-sheet formation while the presence of certain amino acid residues, including lysine, asparagine, glutamine, and proline, are known to disrupt and prevent β-sheet formation.[52]

1.6 PR_g peptide-amphiphiles

The Kokkoli group has previously developed a fibronectin-mimetic peptide amphiphile, PR_g PA shown in Figure 1.5, which self-assembles into nanofibers in aqueous environments and forms hydrogels.[53] The PR_g peptide, which specifically binds the $\alpha_5\beta_1$ integrin, contains both the RGDSP cell binding site and the PHSRN synergy site separated by a linker that mimics the separation length of 30-40 Å in the native structure of fibronectin.[4] The linker was also designed to be flexible and to mimic the hydrophobicity and hydrophilicity between the binding and synergy domains in

fibronectin.[54] The PR_g peptide design was modified from that of the PR_b peptide-amphiphile, which as previously been used conjugated to a dialkyl tail for targeted delivery of liposome carriers.[55–60] The GGGSS spacer of PR_g was originally designed to remove and displace the lysine (K) and proline (P) amino acid residues, which are known to inhibit β-sheet interactions, of the PR_b peptide to allow for cylindrical micelle assembly with a single C_{16} tail.[52,53] TEM imaging, infrared spectroscopy, and circular dichroism methods have shown that β-sheet secondary structures are a common characteristic of peptide-amphiphiles which form cylindrical micelle nanofibers.[44,48–50] The β-sheet hydrogen bonding is particularly important between the first four to six amino acid residues closest to the hydrocarbon tail and has been shown to be critical for gelation.[49] The glycine (G) and serine (S) residues in particular, were selected for their small size but neither residue favors β-sheet formation. Nonetheless, the PR_g peptide-amphiphile has been shown to self-assemble in water to form cylindrical micelle nanofibers which bundle to form hydrogels. PR_g hydrogels form after 48 h and have a modulus of 480 Pa.[53] As surfaces, PR_g hydrogels have been shown to support improved cell adhesion, proliferation and ECM production compared to mechanically matched hydrogel surfaces functionalized with full length fibronectin.[61]

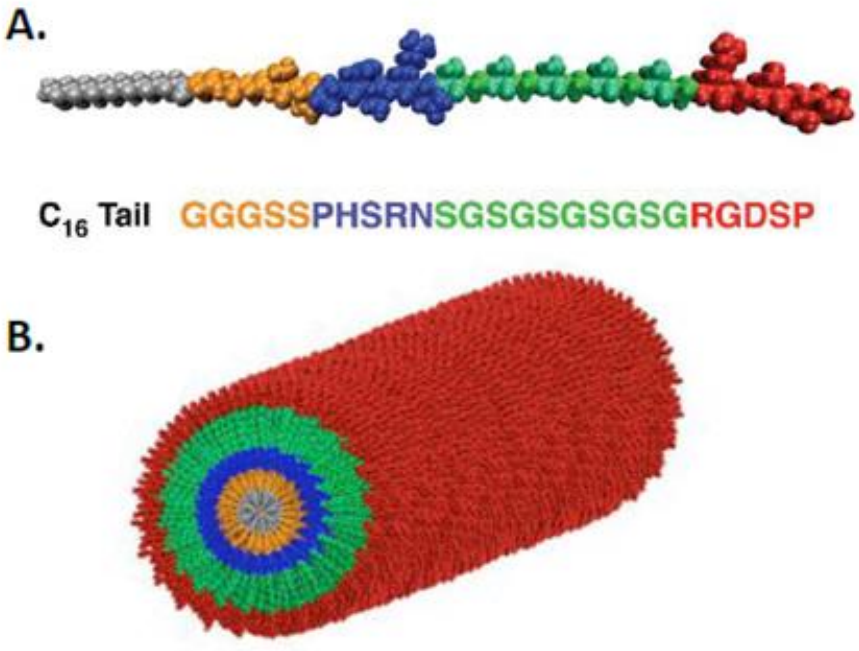

Figure 1.5: (A) PR_g peptide-amphiphile sequence and structure. (B) Schematic of a PR_g nanofiber.

In addition to β-sheet domains, most peptide-amphiphiles which form nanofibers are negatively-charged to facilitate assembly in cell culture media. Some positively-charged peptide-amphiphiles have been reported to assemble into nanofibers in the presence of KCl[62] while others have been shown to co-assemble into nanofibers with negatively-charged peptide-amphiphiles. The PR_g peptide-amphiphile has a charge of +1 at neutral pH. The relatively long time required for PR_g peptide-amphiphiles to self-assemble in water may be due to repulsive electrostatic interactions. The gelation time may be

reduced by introducing negatively-charged electrolytes or peptide-amphiphiles to screen charges on the PR_g peptide-amphiphile.

Chapter 2 3D Cell Entrapment as a Function of the Weight Percent of Peptide-Amphiphile Hydrogels

2.1 Summary

The design of scaffolds which mimic the stiffness, nanofiber structure, and biochemistry of the native extracellular matrix (ECM) has been a major objective for the tissue engineering field. Furthermore, mimicking the innate three dimensional (3D) environment of the ECM has been shown to significantly alter cellular response compared to traditional two dimensional (2D) culture. We report the development of a self-assembling, fibronectin-mimetic, peptide-amphiphile nanofiber scaffold for 3D cell culture. To form such a scaffold, 5 mol % of a bioactive PR_g fibronectin-mimetic peptide-amphiphile was mixed with 95 mol % of a diluent peptide-amphiphile (E2) whose purpose was to neutralize electrostatic interactions, increase the gelation kinetics and promote cell survival. Atomic force microscopy verified the fibrilar structure of the gels and the mechanical properties were characterized for various weight percent (wt %) formulations of the 5 mol % PR_g - 95 mol % E2 peptide-amphiphile mixture. The 0.5 wt % formulations had an elastic modulus of 429.0 ± 21.3 Pa while the 1.0 wt % peptide-amphiphile hydrogels had an elastic modulus of 808.6 ± 38.1 Pa. The presence of entrapped cells in the gels decreased the elastic modulus by approximately 40% for both

the 0.5 and 1.0 wt % peptide-amphiphile hydrogels. While both formulations supported cell proliferation, the 0.5 wt % gels supported significantly greater NIH3T3/GFP fibroblast cell proliferation throughout the gels than the 1.0 wt % gels. However, the 1.0 wt % hydrogels promoted greater increase in expression of fibronectin and type IV collagen ECM protein mRNA compared to the 0.5 wt % formulations. This study suggests that this fibronectin-mimetic scaffold holds great promise in the advance of 3D culture applications and cell therapies.

2.2 Introduction

The importance of the mechanical, structural, and biochemical properties of the native ECM has been recognized and has led to the development of new techniques and chemistries to form and functionalize scaffolds for cell culture. In addition to designing scaffolds which mimic the nanofibrous structure, stiffness and biochemical signals of the ECM, mimicking the innate 3D environment of the ECM has been shown to be critically important for tissue engineering applications.[63–66] Traditional 2D cell culture introduces an artificial polarity between cells' upper and lower surfaces resulting in non-native cell morphologies and receptor and protein expression profiles.[31] Additionally, significant differences in the expression of integrins and other cell surface receptors between 2D and 3D environments have been reported.[34,67]

Encapsulation of cells within a 3D scaffold is most effectively accomplished by introducing cells during gelation in order to ensure uniform cell distribution. Many of the common hydrogel systems currently used for 3D cell entrapment require low pH, as with PuraMatrix;[68] low temperature, as with collagen and Matrigel;[69] or exposure to UV light to initiate gelation, as with polyethylene glycol (PEG),[70,71] which can damage cells and lead to cell death. Peptide-amphiphiles are an attractive material for the design of cell scaffolds which mimic the ECM due to their ability to self-assemble into nanofibrous hydrogels and incorporate relevant bioactive, biomimetic peptide sequences.[72] Peptide-amphiphiles have been shown to form hydrogels in cell culture media and have been used as 3D scaffolds for a variety of applications, including the culture and differentiation of dental stem cells,[73,74] mesenchymal stem cells,[75–77] neural progenitor cells,[14,78,79] cartilage,[80] and pancreatic islets.[81,82] It has been demonstrated that RGD-containing peptide-amphiphile scaffolds support enhanced proliferation and osteogenic differentiation of mesenchymal stem cells compared to peptide-amphiphile scaffolds without the RGD peptide.[76] Peptide-amphiphiles containing the laminin mimetic peptide, IKVAV, have been shown to support neuron differentiation of neural progenitor cells.[14] Peptide-amphiphiles gels have also been shown be biocompatible *in vivo*, with significant degradation within the first 30 days of implantation, followed by completely degrading after 60 days with no signs of acute or chronic inflammation.[83] Other work has shown that entrapped cells internalize the peptide-amphiphile nanofibers and possibly utilize peptide-amphiphiles in their metabolic pathways.[62]

We have previously developed a fibronectin-mimetic peptide-amphiphile, called PR_g, which self-assembles in water to form nanofibrous hydrogels.[53] The PR_g peptide contains both the primary cell binding site, RGD, as well as the PHSRN synergy site. These two sites are separated by a linker which accurately mimics the distance and the overall hydrophobicity/hydrophilicity between these binding domains in fibronectin.[42,54] We have previously demonstrated that the PR_g peptide specifically binds the $\alpha_5\beta_1$ integrin[54] with a dissociation constant of 76.3 ± 6.3 nM.[84] PR_g peptide-amphiphile hydrogels have been shown to support increased cell adhesion, proliferation, and ECM secretion as 2D substrates compared to PEG hydrogels functionalized with fibronectin and PuraMatrix hydrogels.[61]

Electrolytes or diluent peptide-amphiphiles of opposite charge have been used before in the literature to screen charges and enable faster gelation.[44,62] In the absence of any electrolytes or other amphiphiles, PR_g peptide-amphiphiles were prepared in Milli-Q water and aged for 48 h at room temperature before use for our 2D studies.[61] In order to translate our PR_g hydrogels from 2D to 3D, a diluent peptide-amphiphile, E2 (C_{16}-GGGSSSESE), was designed to screen charges on the PR_g peptide-amphiphile (C_{16}-GGGSSSPHSRN$(SG)_5$RGDSP) and facilitate faster gelation (30 min to 1 h at room temperature or 37 °C in Milli-Q water with $CaCl_2$ or in cell culture media).

The goal of this study is to investigate cell responses to changes in weight percentages (wt %) of a hydrogel composed of a mixture of PR_g and E2 peptide-amphiphiles. Given

the amount of evidence in the literature which shows that 5 mol % of an RGD-containing peptide is optimal, or at least sufficient, to facilitate cell adhesion and survival,[85–91] a hydrogel formulation containing 5 mol % PR_g peptide-amphiphile and 95 mol % E2 peptide-amphiphile (PR_g/E2) was chosen for this study. Here we characterize the hydrogel microstructure and mechanical properties of 0.5 and 1.0 wt % PR_g/E2 peptide-amphiphile hydrogels in the presence or absence of entrapped cells, as well as their ability to support cell survival, proliferation and ECM expression in a 3D environment.

2.3 Experimental methods

2.3.1 Materials

All chemicals were purchased from Thermo Fisher Scientific except otherwise stated. Atomic force microscopy contact mode rectangular Si cantilevers with an Al-coated backside (NSC36/Al BS) were acquired from MikroMasch (Lady's Island, SC). Ruby mica sheets, V2 quality, were purchased from S&J Trading Inc. (Glen Oaks, NY). Water, purified to a resistivity of 18.2 MΩ/cm, was obtained from a Milli-Q water system (EMD Millipore, Billerica, MA) and sterilized by autoclaving before using it to prepare hydrogels. NIH3T3/GFP fibroblasts were purchased from Cell Biolabs Inc. (San Diego, CA) and Dulbecco's modified Eagle medium (DMEM) from Life Technologies (Grand Island, NY).

2.3.2 Synthesis of peptide-amphiphiles

The protected PR_g peptide (GGGSSSPHSRN$(SG)_5$RGDSP) and E2 diluent peptide (GGGSSESE) were synthesized by the Oligonucleotide and Peptide Synthesis Facility at the University of Minnesota using standard Fmoc solid phase synthesis on peptide amide linker resin. The Fmoc protecting group was removed using a solution of 20% piperidine in dimethylformamide (DMF). A palmitic acid, C_{16}, tail was coupled to the N-terminus of the peptide with 4.5 molar equivalents of N,N,N′,N′-Tetramethyl-O-(1H-benzotriazol -1-yl)uronium hexafluorophosphate (HBTU), 4.5 molar equivalents of palmitic acid, and 6 molar equivalents of diisopropylethylamine in DMF for 4 h. The Kaiser test was used to verify complete coupling of the tails to the peptide amide. The resin beads were washed twice in DMF, dichloromethane, and methanol and dried overnight under vacuum. Peptide-amphiphiles were cleaved from resin in a cleavage cocktail of 90% trifluoroacetic acid (TFA), 5% thioanisole, 3% 1,2-ethandithiol, and 2% anisole for 2 h. The solution was collected and precipitated in 20X excess cold isopropyl ether. The precipitate was collected by centrifugation (10 min at 7,000 RCF), redissolved in Milli-Q water and purified using reversed phase high performance liquid chromatography (HPLC) on an Agilent 1100 Series system with a Waters Xterra Prep MS C18 column, using a water/methanol gradient with 0.1% TFA for PR_g or 0.1% ammonium hydroxide for E2. The pure peptide-amphiphile product was analyzed with the Bruker BioTOF II to verify that the product had the expected mass. Peptide-amphiphiles were stored as

lyophilized powder at -20 °C. Stock solutions of peptide-amphiphiles were prepared in Milli-Q water from the lyophilized peptide-amphiphiles and aliquots were stored at -20 °C to avoid freeze-thaw. All peptide-amphiphile gels in this study contained 5 mol % PR_g and 95 mol % E2. Specifically, gels contained 0.24 mM PR_g and 4.4 mM E2 or 0.48 mM PR_g and 8.8 mM E2 for the 0.5 wt % and 1.0 wt % gels respectively.

2.3.3 Atomic force microscopy (AFM)

2X concentrations of peptide-amphiphile solutions containing 5 mol % PR_g and 95 mol % E2 were mixed with an equal volume of DMEM media supplemented with 10 mM $CaCl_2$ on 15 mm mica discs. Gels were allowed to dry for 5 days at room temperature in a laminar flow hood or at 37 °C. AFM imaging of the dehydrated samples was performed with a Nanoscope V Multimode 8 SPM (Bruker, Santa Barbara, CA) in contact mode in air using rectangular Si cantilevers with a typical probe tip radius of 8 nm.

2.3.4 Rheology

The mechanical properties of peptide-amphiphile hydrogels with and without cells were characterized using an AR-G2 rheometer from TA Instruments. 2X concentrations of peptide-amphiphile solutions containing 5 mol % PR_g and 95 mol % E2 were loaded onto the peltier plate and mixed with an equal volume of DMEM media supplemented with 10 mM $CaCl_2$. For the gel characterization with the entrapped cells, 2X concentrations of peptide-amphiphile solutions containing 5 mol % PR_g and 95 mol %

E2 were loaded onto the peltier plate and mixed with an equal volume of DMEM media supplemented with 10 mM $CaCl_2$ containing 2.7 x 10^6 or 1.35 x 10^6 cells/mL. Immediately after mixing, the 8 mm parallel plate was lowered to a gap of 500 μm for the gels without the cells, or to a gap of 1,000 μm for the gels with the cells, and the peltier plate was heated to 37 °C. The gels were allowed to mature in a hydrated chamber for 2 h before frequency sweep measurements were made from 0.1 to 10 rad/s at 1% strain. Strain sweeps performed prior to frequency sweeps showed that 1% strain fell within the linear viscoelastic regime. For time sweep experiments, gels were prepared with and without cells as described above and coated with low viscosity oil (dimethylpolysiloxane) to prevent dehydration.

2.3.5 Cell culture

NIH3T3 fibroblasts expressing green fluorescent protein (GFP), NIH3T3/GFP, were cultured in DMEM supplemented with 0.1 mM non-essential amino acids, 100 units/mL penicillin, 100 μg/mL streptomycin, 10 μg/mL blasticidin (Life Technologies, Grand Island, NY), and 10% fetal bovine serum (FBS) (Atlas Biologicals, Fort Collins, CO). NIH3T3 fibroblasts were cultured in DMEM supplemented with 100 units/mL penicillin, 100 μg/mL streptomycin and 10% FBS. Media was changed every 2-3 days until cells reached confluency and were passaged. Cells were used between passage 3 and 7.

2.3.6 Cell viability and proliferation assays

Gels (0.5 wt % and 1.0 wt %) were prepared from peptide-amphiphile stock solutions in Milli-Q water. Concentrated (2X) peptide-amphiphile solutions were mixed with an equal volume of cell (NIH3T3/GFP or NIH3T3) suspension containing 2.7 x 10^6 cell/mL in complete DMEM media supplemented with 10 mM $CaCl_2$. The final concentration of the entrapped cells in the gel was 1.35 x 10^6 cells/mL. The peptide-amphiphile gels were allowed to mature at 37 °C for 1 h before DMEM media without $CaCl_2$ was added to the top of the gels. Media was replenished every 2 days. For the live/dead assay, viability was examined at 24 h and 5 day time points using the Live/Dead® Viability/Cytoxicity Kit (Invitrogen, Grand Island, NY) following the manufacturer's instructions. Imaging was done on a Ziess Cell Observer SD Spinning Disk Confocal at the University Imaging Center at the University of Minnesota and cells were maintained at 37 °C with 5% CO_2. GFP cell fluorescence was quantified using a Biotek Synergy H1 plate reader (Winooski, VT) with a 485/528 filter. The background from gels without cells was subtracted from all measurements, and fluorescence was normalized to the 3 h time point. The persistence of GFP fluorescence in dead cells was examined using fluorescence microscopy. NIH3T3/GFP fibroblasts were plated in 96-well plates at a density of 250 cells/mm^2 and were allowed to adhere overnight. Attached fibroblasts were imaged using transmitted light and the GFP cube (Ex: 470 nm, Em: 525 nm) on an EVOS FL microscope (Life

Technologies, Grand Island, NY). Ethanol (30%) was added to wells and cells were imaged again after 5 min.

2.3.7 Real-time reverse transcription polymerase chain reaction (RT-PCR) for ECM mRNA

RNA was extracted from the 1.35 x 10^6 NIH3T3/GFP cells/mL gels 3 h after encapsulation on day 0 and on day 5 of culture using the E.Z.N.A.® Total RNA Kit I (Omega Biotek, Norcross, GA). The reverse transcription to cDNA was done with qScript cDNA SuperMix (Quanta Biosciences, Gaithersburg, MD) following the manufacturer's instructions. Primers for fibronectin (FN1), collagen IV (Col4α1, Col4α2, Col4α3), and housekeeping gene glyceraldehyde 3-phosphate dehydrogenase (GAPDH) were designed using the NCBI primer blast tool (Table 2.1). Real-time RT-PCR was done in 25 μL reactions following manufacturer's instructions using PerfeCTa SYBR Green, Low ROX (Quanta Biosciences, Gaithersburg, MD) and a Stratagene Mx3000P system.

2.3.8 Histology and immunohistochemistry

NIH3T3/GFP (1.35 x10^6 cells/mL) entrapped for 5 days in 0.5 and 1.0 wt % gels were fixed for 15 min in 4% paraformaldehyde in tris-buffered saline (TBS) and then washed 3 times in TBS. Fixed gels were submitted to the histology and immunohistochemistry lab at the University of Minnesota. HistoGel (Richard-Allan Scientific, Kalamazoo, MI) was

used according to the manufacturer's protocol to protect the gel samples during processing. Unstained cell block sections (4 μm) were deparaffinized and rehydrated using standards methods. For antigen retrieval, slides were incubated in Reveal Decloaking Reagent, pH 6.0, in a steamer at 95-98℃ for 30 min and then cooled for 20 min. Slides were rinsed in tap water and immersed in TBS/0.1% triton (TBST). Slides were placed in the Nemesis 7200 (Biocare Medical, Concord, CA) and endogenous peroxidase activity was quenched by immersing slides in Peroxidazed 1, a 3% hydrogen peroxide solution, for 10 min followed by a TBST rinse. Sections were blocked for 30 min in a serum-free blocking solution (Background Sniper, Biocare Medical, Concord, CA) before application of diluted primary antibodies in 10% blocking solution/ 90% TBST for 1 h at room temperature. Anti-fibronectin- (1:200, Abcam, Cambridge, MA) or anti-collagen IV- (1:200, Millipore, Temecula, CA) stained slides were rinsed in TBST and Novolink post primary (Leica Microsystems, Buffalo Grove, IL) was applied for 30 min at room temperature. Slides were rinsed in TBST followed by Novolink polymer (Leica Microsystems, Buffalo Grove, IL) for 30 min at room temperature, rinsed again in TBST, and incubated in CAT Hematoxylin (BioCare Medical, Concord, CA) for 5 min. Slides were rinsed in Milli-Q water, dehydrated using standard methods, cover slipped, and imaged using a Leica DME light microscope.

Table 2.1: Forward (F) and reverse (R) primer sequences for fibronectin (FN1), Collagen IV (Col4α1, Col4α2, Col4α3), and housekeeping gene GAPDH.

Gene		Primer Sequence
FN1	F	GCCACCATTACTGGTCTGGA
	R	GGTTGGTGATGAAGGGGGTC
Col4α1	F	TTAGCAGGTGTGCGGTTTGT
	R	GGCGAGCCAAAAGCTGTAAG
Col4α2	F	CGGCGTAATCTCAAAAGGCG
	R	GGCCTCTGCTTCCTTTCTGT
Col4α3	F	GAGAACCATCCGTAGGCAGG
	R	CTTCGACCTGGTTGCCCTTT
GAPDH	F	GAAACCTGCCAAGTATGATGACA
	R	CTTGCTCAGTGTCCTTGCTG

2.4 Results and Discussion

2.4.1 Hydrogel microstructure

Pure PR_g hydrogels result from the self-assembly of the amphiphiles in water to form nanofibers and further aggregation of the nanofibers into a network of bundles as shown by cryogenic transmission electron microscopy (cryo-TEM) evaluation of PR_g samples.[24] The nanoscale surface morphology of the pure PR_g peptide-amphiphile hydrogels was investigated with scanning electron microscopy (SEM) and cryo-SEM and verified the nanofibrous network structure of the PR_g hydrogels and the presence of

fiber bundles.[28] In this work AFM was used to evaluate the surface morphology of PR_g/E2 gels for the 0.5 wt % and 1.0 wt % hydrogels (Figure 2.1). Gels were left to dry at room temperature or at 37 °C and AFM images were collected in air. Results showed that the method of dehydration had no effect on the surface topography. Figure 2.1 verified the nanofibrous structure of the PR_g/E2 gels and the presence of bundles of nanofibers that varied in diameter between 50-130 nm for both wt %, in agreement with our previous PR_g cryo-TEM images.[24]

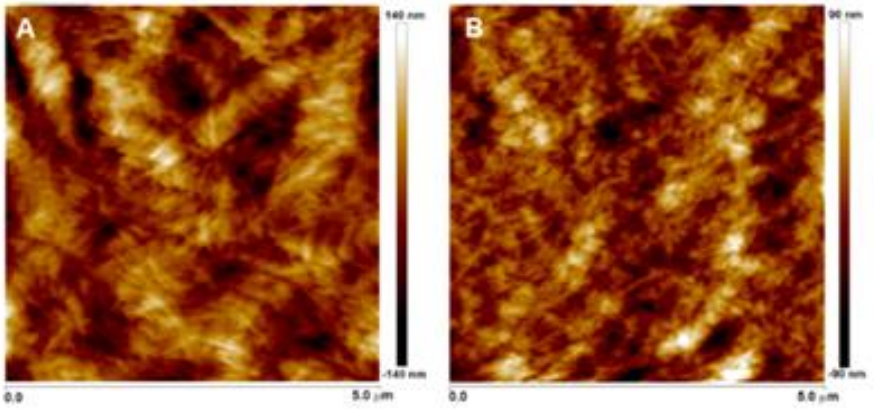

Figure 2.1: AFM images (5 µm X 5 µm) in air of 5 mol% PR_g-95 mol % E2 peptide-amphiphile hydrogels at (A) 0.5 wt % and (b) 1.0 wt %.

2.4.2 Rheology

The mechanical properties of 0.5 wt % and 1.0 wt % PR_g/E2 hydrogels were measured using oscillatory rheology (Figure 2.2). Both gel formulations have a storage modulus (G') greater than the loss modulus (G"), indicating that they do in fact form gels. Frequency sweeps in Figure 2.2 show that both hydrogels have minimal frequency

dependence, indicating that there is a high degree of physical crosslinking. Because the measurement of storage and loss moduli were obtained in the linear viscoelastic regime, the elastic modulus, E, can be calculated by the following equation:

$$E = 3 * \sqrt{G'^2 + G"^2}$$

The elastic modulus of the 0.5 wt % gels was 429.0 ± 21.3 Pa and the elastic modulus of the 1.0 wt % gels was almost twice the modulus of 0.5 wt % gels, at 808.6 ± 38.1 Pa.

Rheological characterization of peptide-amphiphile hydrogels with entrapped cells (Figure 2.3) revealed that the presence of cells decreased the elastic modulus, and the decrease was a function of the cell loading (Figure 2.4). As Figure 2.4 shows, the entrapment of 1.35 x 10^6 NIH3T3/GFP cells/mL decreased the elastic modulus by approximately 40%, to 256.8 ± 8.7 Pa and 491.9 ± 35.2 Pa for the 0.5 wt % and 1.0 wt % hydrogels respectively. The modulus of adherent cells has been reported to be between 30 Pa and 150 Pa when measured magnetic twisting cytometry and optical tweezers.[92,93] Much higher cell moduli have been reported from atomic force microscopy (AFM) measurements, although there is evidence to suggest that the substrate on which the cells are adhered and the state of adherence can significantly alter these measurements.[94] The observed decrease in modulus after cell encapsulation may be a result of encapsulating cells that are softer than the gel; however, it is more likely due to the disruption of physical interactions between nanofibers and nanofiber bundles. This is the first evidence

in the peptide-amphiphile literature showing the drastic changes in mechanical properties of the gel as a result of cell entrapment. While others have reported a dependence of the modulus on the concentration of the hydrogel solution for physical hydrogels used for cell culture,[29,95,96] these measurements were typically made in the absence of cells. Our results indicate that the effect of cell encapsulation on the modulus of a physical hydrogel is more significant than previously thought.

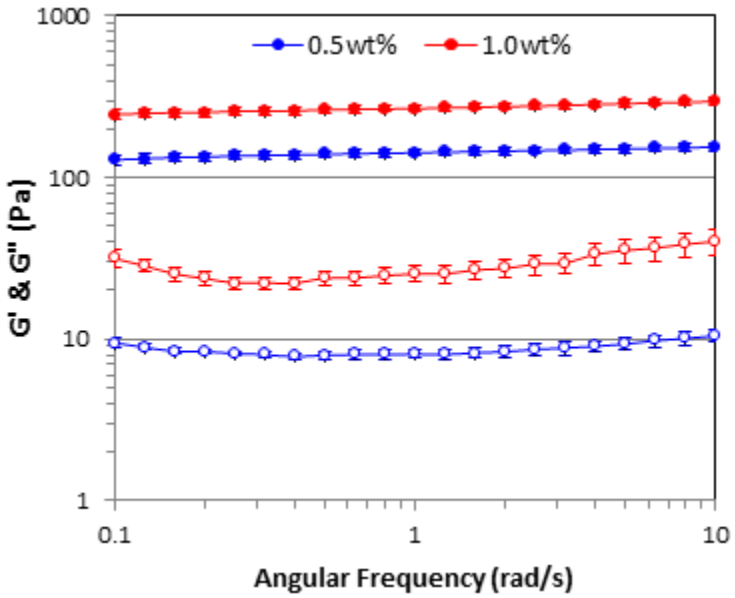

Figure 2.2: Rheology of 5 mol% PR_g-95 mol % E2 peptide-amphiphile hydrogels. Data are shown as the mean ± standard error from three independent experiments (*n*=3). Filled symbols represent the storage modulus (G'), and open symbols represent the loss modulus (G").

Time sweep experiments were performed to determine how the hydrogel modulus changes over time in the presence and absence of cells. Technical challenges, including sample dehydration (even though samples were coated with low-viscosity oil to prevent dehydration) and loss of contact between the hydrogel and the parallel plate, prevented measurement for 5 days. For the 42 to 65 h for which data could be collected, no changes in hydrogel modulus were observed (Figure 2.5). These results indicate that the hydrogels do not degrade or lose mechanical integrity during the time examined.

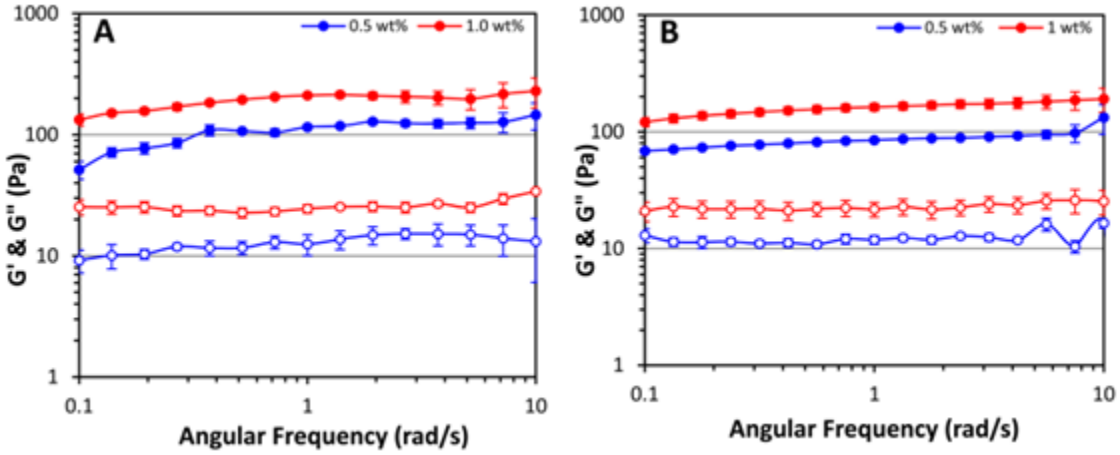

Figure 2.3: Rheology of 5 mol% PR_g – 95 mol % E2 peptide-amphiphile hydrogels containing (A) 6.75 X 10^5 NIH3T3/GFP fibroblasts per mL, and (B) 1.35 X 10^6 NIH3T3/GFP fibroblasts per mL. Data are shown as mean ± standard error from three independent experiments (*n*=3). Filled symbols represent the storage modulus (G") and open symbols represent the loss modulus (G").

Both the 0.5 wt % and 1.0 wt % gels, with and without cells, have appropriate moduli to be used as scaffolds for tissue engineering applications, falling within the range of elastic moduli of soft tissue, 100 and 10,000 Pa.[23,97] In particular, hepatic and pancreatic applications would be appropriate for our hydrogel system, with moduli between 400-600 Pa[98] and between 640-1160 Pa[99] respectively.

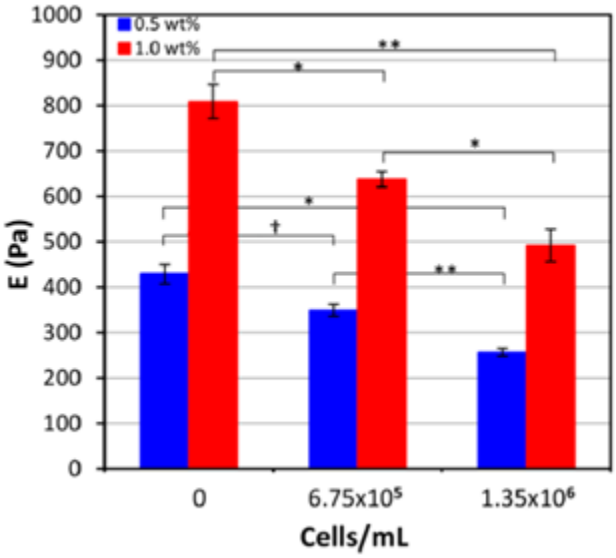

Figure 2.4: Elastic modulus of 5 mol % PR_g – 95 mol % E2 peptide-amphiphile hydrogels as a function of NIH3T3/GFP cell loading. Data are shown as the mean ± standard error from three independent experiments (*n*=3). ANOVA analysis was performed, and the statistical significance noted for the bracketed data (* $p < 0.05$, ** $p < 0.005$, † $p > 0.05$).

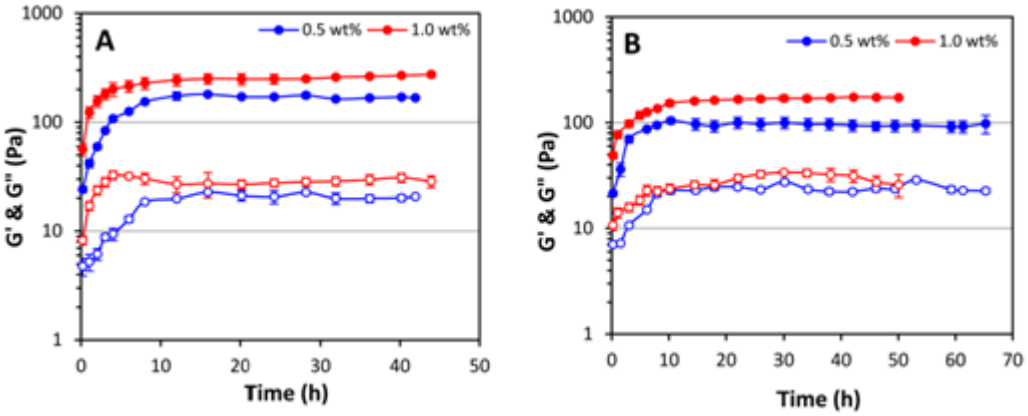

Figure 2.5: Rheology of 5 mol % PR_g – 95 mol % E2 peptide-amphiphile hydrogels (A) without and (B) with entrapped 1.35 X 10^6 NIH3T3/GFP fibroblasts/mL. Data are shown as the mean ± standard deviation from two independent experiments (*n*=2). Filled symbols represent the storage modulus (G") and open symbols represent the loss modulus (G").

2.4.3 Cell viability and proliferation within peptide-amphiphile hydrogels

NIH3T3/GFP fibroblasts were selected in order to easily visualize cells within our hydrogel constructs and to avoid other methods of measuring cell viability and proliferation which can be complicated by limited diffusion through the gels and high background signals from the gels themselves. Live cells expressing GFP could be readily observed within the PR_g/E2 gels using confocal microscopy, and z-stacks were collected at 3, 24, 48, 72 h and 5 days. After 3 and 24 h, cells appeared to be rounded with little spreading apparent in both the 0.5 wt % and the 1.0 wt % PR_g/E2 gels (Figure 2.6). This observation differs from previously reported behavior of cell attachment and spreading on 2D PR_g hydrogels, where cells were able to attach and spread within the

first 24 h.[61] In a 3D environment, cells appear to require more time to attach and spread. This is consistent with reports that cells embedded in a 3D matrix must first remodel their ECM before spreading, migrating, or depositing their own ECM.[100–103] After 48 h, an increase in cell number was observed (Figure 2.8) as well as cell clusters or aggregates, with larger clusters observed in the 0.5 wt % versus the 1.0 wt % gel (Figure 2.6). We hypothesize that the clustering is likely a result of cell proliferation. At both 72 h and 5 days cell number continues to increase (Figure 2.8) along with the size of the cell clusters (Figure 2.6), with more and larger cell clusters observed in the 0.5 wt % gels. Higher magnification images of cells at 24 h and 5 days in the 0.5 wt % and the 1.0 wt % PR_g/E2 gels are shown in Figure 2.7.

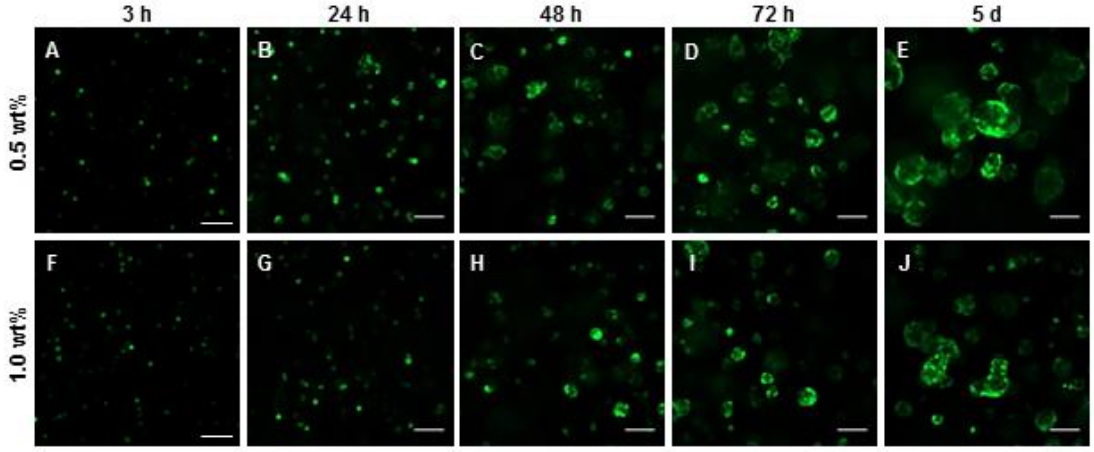

Figure 2.6: Representative confocal images of NIH3T3/GFP fibroblasts in 5 mol % PR_g – 95 mol % E2 peptide-amphiphile hydrogels over time. Images shown are 100 µm above the bottom of the well and 900 µm below the surface of (A-E) 0.5 wt% gels and (F-J) 1.0 wt % gels. NIH3T3/GFP fibroblasts are shown in green. The scale bars is 100 µm for all images.

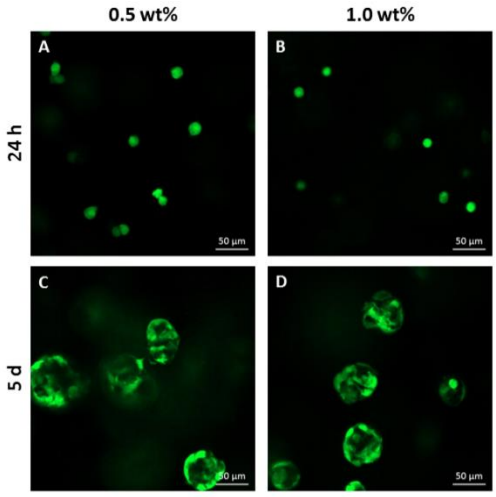

Figure 2.7: Confocal images of NIH3T3/GFP fibroblasts in 5 mol % PR_g – 95 mol % E2 peptide-amphiphile hydrogels. Images shown are from 0.5 wt % and 1.0 wt % gels after 24 h (A, B) and 5 days (C, D). NIH3T3/GFP cells are shown in green.

The quantification of GFP fluorescence in Figure 2.8 from the 0.5 wt % gels was statistically significantly higher than the fluorescence from the 1.0 wt % gels at 48 h, 72 h, and 5 days (p-values from ANOVA analysis of all the fluorescent data can be found in Table 2.2 and Table 2.3). Confocal images combined with the fluorescence quantification indicate that cells within the 0.5 wt % gels proliferate more compared to cells within the 1.0 wt % gels. The observed increase in proliferation in the lower modulus gel formulation is consistent with observations of fibroblasts encapsulated in 3D protein scaffolds and polymer hydrogels.[104,105] For example, a lower protein wt % resulted in increased porosity and interconnectivity within scaffolds which has been associated with cell migration within porous 3D protein scaffolds, allowing more cells to proliferate, this

reducing cell death due to overcrowding.[104] These results are also consistent with the suggestion that highly crosslinked hydrogels and gels with lower porosity make it more difficult for cells to spread and proliferate in three dimensions.[105,106] In particular, it has been shown that the proliferation and spreading of fibroblasts encapsulated in PEG hydrogels functionalized with RGD-containing peptide increased with decreasing material stiffness.[105] It was suggested that gels with higher stiffness pose an increased physical barrier and confinement, thus impairing cell proliferation in 3D environments. The higher the modulus, the denser the gel scaffold surrounding the cells and the smaller the space for the cell to proliferate, spread, and migrate.[105]

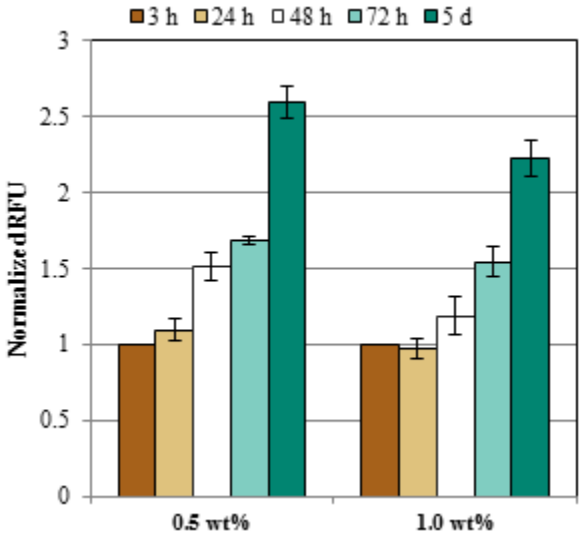

Figure 2.8: Fluorescence quantification of NIH3T3/GFP fibroblasts entrapped in 5 mol % PR_g – 95 mol % E2 hydrogels over time. Data described are the relative fluorescence unit (RFU) detected from the GFP-expressing cells normalized to the 3 h time point. Data are shown as the mean ± standard error from four independent experiments (*n*=4) done in triplicate.

Table 2.2: p-values from the ANOVA analysis of fluorescence signal from the NIH3T3/GFP fibroblasts entrapped in 0.5 or 1.0 wt % of PR_g/ E2 peptide-amphiphile hydrogels over time.

0.5 wt% Gels					
	3 h	**24 h**	**48 h**	**72 h**	**5 days**
3 h		> 0.05	< 0.001	< 0.001	< 0.001
24 h			< 0.001	< 0.001	< 0.001
48 h				< 0.05	< 0.001
72 h					< 0.001
5 days					
1.0 wt% Gels					
	3 h	**24 h**	**48 h**	**72 h**	**5 days**
3 h		> 0.05	< 0.05	< 0.001	< 0.001
24 h			< 0.05	< 0.001	< 0.001
48 h				< 0.01	< 0.001
72 h					< 0.001
5 days					

Table 2.3: p-values from the ANOVA analysis of fluorescence signal from the NIH3T3/GFP fibroblasts entrapped in 0.5 wt % or 1.0 wt % of 5 mol % PR_g – 95 mol % E2 peptide-amphiphile hydrogels over time.

0.5 wt% *vs.* 1.0 wt% Gels	
3 h	> 0.05
24 h	> 0.05
48 h	< 0.01
72 h	< 0.05
5 days	< 0.01

Quantification of cell viability via GFP fluorescence has been demonstrated in the literature previously. The half-life of GFP in NIH3T3 fibroblasts is 2.8 h,[107] and decreases in fluorescence intensity have been shown to correlate well with traditional

apoptosis and necrosis assays.[108] GFP fluorescence in dead cells returned to background levels and was indistinguishable from the autofluorescence of the live cells.[109] Thus, it has been demonstrated that the loss of GFP fluorescence parallels the loss of cell viability in NIH3T3 fibroblast cells.[109] We also examined cell viability via other methods. First, the GFP fluorescence of dead cells was evaluated and was shown to decrease rapidly (Figure 2.9), in agreement with literature findings,[109] demonstrating that the GFP fluorescence of the entrapped cells in Figure 2.6 and Figure 2.8 comes from live cells. The live/dead cell viability assay was also used on NIH3T3 cells (without the GFP plasmid) encapsulated in 0.5 wt % and 1.0 wt % PR_g/E2 gels after 24 h and 5 days (Figure 2.10). After 24 h, there was some cell death following the initial cell entrapment, as both green and red cells were observed. However, after 5 days only green cells were observed indicating that there was no additional death among cells that survived the initial entrapment.

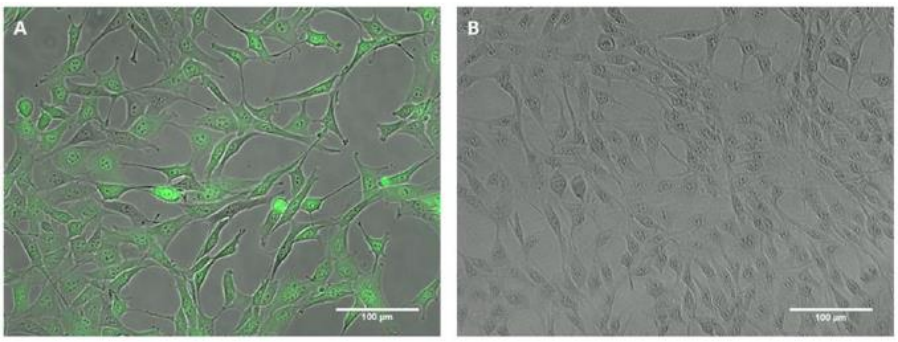

Figure 2.9: Fluorescence overlay on phase images of NIH3T3/GFP fibroblasts. (A) Live cells and (B) cells killed after exposure to 30% ethanol for 5 min.

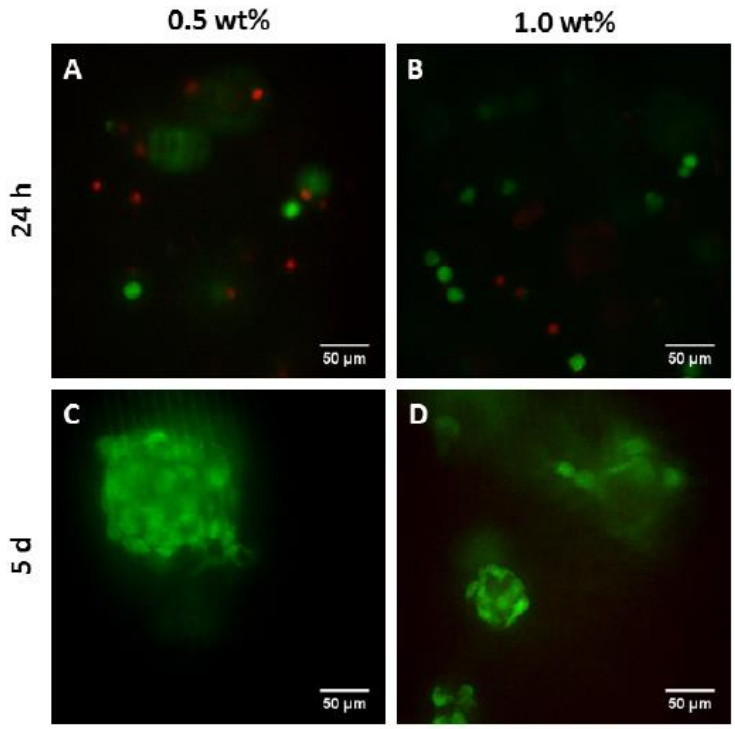

Figure 2.10: Confocal images of NIH3T3 fibroblasts entrapped in 5 mol % PR_g – 95 mol % E2 peptide-amphiphile hydrogels and evaluated with the Live/Dead cell viability assay. Both 0.5 wt % and 1.0 wt% gels were examined at 24 h (A, B) and 5 days (C, D). Green cells are alive and red cells are dead.

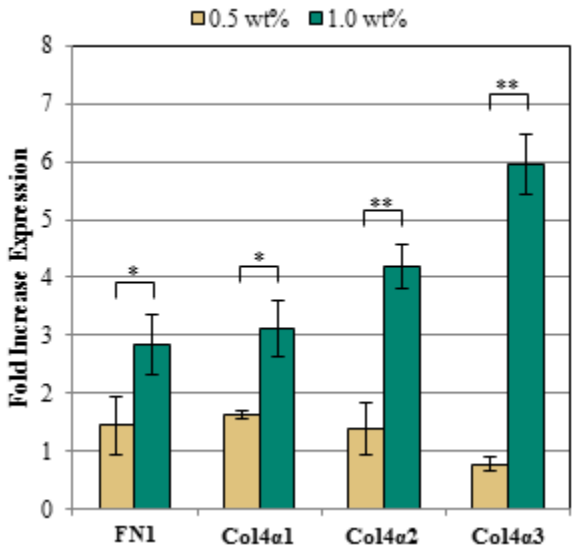

Figure 2.11: Real-time PCR results of ECM mRNA expression from the NIH3T3/GFP fibroblasts entrapped in 5 mol % PR_g – 95 mol % E2 hydrogels. The fold increase in expression compares 3 h and day 5 expression of fibronectin (FN1) and collagen IV (Col4α1, Col4α2, Col4α3). Data are shown as mean ± standard error from four independent experiments (*n*=4) done in triplicate. Statistical analysis was performed using a one-sided t test, and the significance in noted for bracketed data (* $p < 0.05$; ** $p < 0.01$).

2.4.4 Real-time RT-PCR for ECM mRNA

Real-time RT-PCR was used to measure the expression of ECM mRNA produced by the NIH3T3/GFP cells entrapped in the 0.5 and 1.0 wt % PR_g/E2 hydrogels. After 5 days of culture, an increase in the expression of fibronectin and type IV collagen was observed for both gel concentrations (Figure 2.11). A previous study has also shown an increase in collagen ECM expression over time after osteogenic differentiation of dental pulp stem cells encapsulated in a matrix metalloproteinase-sensitive, RGD-functionalized peptide-

amphiphile scaffold.[73] The mechanical properties of polymeric hydrogels have been shown before to influence ECM production in different ways, and increased cell proliferation has been frequently correlated with decreased ECM synthesis, as seen in our study.[110–112] This is the first study that shows that cells within the 1.0 wt % peptide-amphiphile hydrogel had significantly higher expression of fibronectin and type IV collagen (α1, α2, and α3 isoforms) compared to the 0.5 wt % peptide-amphiphile gels. It has previously been shown that the α3 isoform of type IV collagen plays a critical role in the assembly of stable collagen IV molecules and that increased expression of the α3 occurs simultaneously with collagen IV protein deposition.[113,114] The significant increase in the α3 isoform of collagen IV in the 1.0 wt % gels over time and compared to the 0.5 wt % samples is likely indicative of more fibril collagen IV protein in the ECM of the cells entrapped in the 1.0 wt % gels.

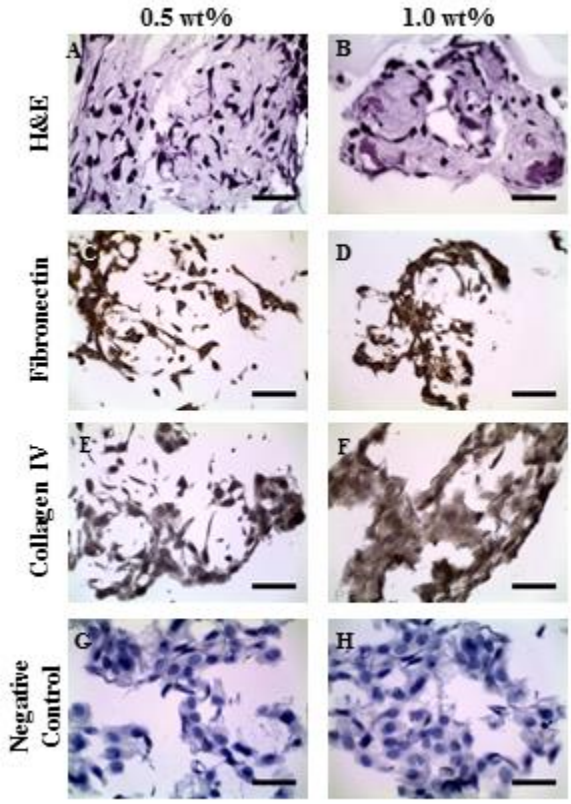

Figure 2.12: Histological and immunohistochemical evaluation of 1.35 X 10^6 NIH3T3/GFP cells/mL entrapped for 5 days in 0.5 and 1.0 wt % hydrogels of 5 mol % PR_g – 95 mol % E2 peptide-amphiphiles. H&E stain (A, B), fibronectin stain (C, D), collagen IV stain (E, F), and a negative control without primary antibodies (G, H). The scale bar is 50 μm for all images.

2.4.5 Histology and immunocytochemistry

Haemotoxylin and eosin (H&E) staining revealed that NIH3T3/GFP fibroblasts in both the 0.5 wt % and 1.0 wt % gels were still associated with the hydrogel matrix after 5 days of culture (Figure 2.12 A, B). Cell clusters are visible in both 0.5 wt % and 1.0 wt % gel, consistent with the results of Figure 2.6. Immunohistochemistry revealed the presence of

fibronectin (Figure 2.12 C,D) and collagen IV (Figure 2.12 E,F) ECM proteins. A negative control without primary antibodies (Figure 2.12 G,H) shows that the fibronectin and collagen IV staining are specific. The 1.0 wt % gels appear to have more collagen IV and fibronectin compared to the 0.5 wt % gels, which is consistent with the observed increase in mRNA expression shown in Figure 2.11.

2.5 Conclusions

A peptide-amphiphile hydrogel was designed using the fibronectin-mimetic PR_g peptide-amphiphile and the E2 diluent peptide-amphiphile to support 3D cell culture. The hydrogel microstructure and mechanical properties of 0.5 and 1.0 wt % gels were studied and it was found that the elastic modulus increased with higher wt % gels. Even though the presence of entrapped cells decreased the elastic modulus of the gels, the values still fall within the range reported for soft tissue, supporting the potential relevance of these hydrogels as tissue engineering scaffolds. Both 0.5 and 1.0 wt % hydrogels were able to support 3D culture and proliferation of NIH3T3/GFP fibroblasts over a period of five days. Although the 0.5 wt % gels supported significantly higher rates of proliferation after 5 days of culture, the 1.0 wt % gels supported significantly higher mRNA expression and production of ECM proteins. These results show that the PR_g/E2 peptide-amphiphile hydrogels are an effective scaffold for 3D cell culture which has the potential to improve the design of ECM mimetic scaffolds for tissue engineering.

Chapter 3 Multifunctional Peptide-Amphiphile Hydrogels

3.1 Introduction

Functionalization of scaffolds with a single bioactive signal has proven effective to mediate cell adhesion to promote cell survival, but these scaffolds dramatically oversimplify the complexity of the native ECM. By incorporating multiple bioactive peptide-amphiphiles, scaffolds can be designed to better reproduce the complex signaling of the native ECM in a tissue specific manner. In particular, peptide mimetics of collagen I, basic fibroblast growth factor, and a heparin binding sequence were designed as amphiphiles to be combined with the PR_g/E2 hydrogels. The sequences of the newly designed peptide amphiphiles can be found in Table 3.1.

Table 3.1: Peptide-amphiphile sequences.

Peptide	Sequence	Charge
E2	C_{16}-GGGSSSESE	-2
PR_g	C_{16}-GGGSSSPHSRN$(SG)_5$RGDSP	+1
Collagen I	C_{16}-GGGSSSGTPGPQGIAGQRGVV	+1
bFGF	C_{16}-GGGSSSYRSRKYSSWYVALKR	+5
Heparin-binding	C_{16}-GGGSSSLRKKLGKA	+4

3.1.1 Collagen I

Collagens are the most abundant protein, found ubiquitously in the tissues of the body. Collagens tend to form triple helical fibers which serve important structural roles in the ECM and provide tensile strength to tissues. Type IV collagen is found primarily in the basal lamina while type I and type III collagens are common in ECMs and bind to the $\alpha_2\beta_1$ integrin. Several collagen mimetic proteins have been studied in the literature. A type III collagen-mimetic peptide: KOGEOGPK based on the CB4 fragment of the α chain has been studied as soluble coagulation inducing peptides, but no surface functionalization studies or cell adhesion studies have been performed.[115,116] The P-15 peptide, GTPGPQGIAGQRGVV, is a linear peptide derived from the cell binding domain of the α1 chain of type I collagen. P-15 has been shown to competitively bind and block collagen receptors ($\alpha_2\beta_1$ integrin) and increase the expression of metalloproteases in fibroblasts to a similar extent as the full protein.[117] Other type I collagen-mimetic peptides include the DGEA peptide, from residues 435-438 of type I collagen[118,119] and the GOFGER peptide from residues 502-507, where O represents hydroxyproline).[120] The bioactivity of the GOFGER peptide is dependent on the helical structure found in the native protein. As a result, the sequence is surrounded by helix forming sequences: $GGYGGGPC(GPP)_5GOFGER(GPP)_5GPC$.[12] A study comparing these three type I collagen-mimetic peptides showed that the GOFGER helical-peptide failed to stimulate cell adhesion and spreading. While both linear peptides supported cell adhesion and

spreading, the P-15 peptide more effectively blocked the $\alpha_2\beta_1$ integrin and better supported osteogenic differentiation.[16,121] The P-15 peptide was selected for the design of a collagen-mimetic peptide amphiphile because it has the highest specificity to the $\alpha_2\beta_1$ integrin of sequences in the literature and because it is sufficiently small in size and doesn't have a defined secondary structure which could disrupt or be disrupted by peptide-amphiphile assembly.

3.1.2 Basic fibroblast growth factor

Basic fibroblast growth factor (bFGF) is an important mitogenic factor for many cell types, including neurons, hepatocytes, endothelial cells, and stem cells.[122–125] Baird et al identified a peptide sequence YRSRKYSSWYVALKR, from residues 110-120 in native bFGF, which competitively binds to the fibroblast growth factor receptor (FGFR).[126] Lin et al combined this sequence with a heparin binding domain in the F2A branched peptide: YRSRKYSSWYVALKR-**K**-(YRSTKYSSWYVALKR) -Ahx_3-RKRLDRIAR, where Ahx is a synthetic amino acid, aminocaproic acid and the FGFR binding domain repeats branch from the indicated lysine residue.[127] The inclusion of the heparin binding domain had no effect on FGFR affinity, and the branched FGFR domain repeats did not have a significant effect on the mitogenic effect on osteoblasts.[128] Because the more complicated F2A peptide did not provide significant improvement on receptor affinity or mitogenic response, the linear sequence identified by Baird et al. will be used to design bFGF-mimetic peptide-amphiphiles.

3.1.3 Heparin binding

Heparin and heparin sulfates are glycosaminoglycans in the ECM and have the ability to bind many growth factors. Amino acid sequences of the form XBBBXXBX, where B is a basic and X is a non-basic amino acid, are found in many growth factors and have been shown to bind with high affinity to heparin sulfate.[129] Surfaces and scaffolds have been functionalized with low molecular weight heparin and octasaccharides for growth factor binding.[130] Sulfonated tyrosine and lysine containing peptides have been shown to have heparin-like growth factor binding affinities.[131] The LRKKLGKA peptide sequence has been shown to bind heparin and increase binding of vascular endothelial growth factor (VEGF) and bFGF, in scaffolds implanted in rat corneas *in vivo*, resulting in increased angiogenesis.[132,133] The simpler chemistry of the non-sulfonated LRKKLGKA peptide will be used to design heparin-binding peptide-amphiphiles.

3.2 Experimental Methods

3.2.1 Materials

All chemicals were purchased from Thermo Fisher Scientific unless otherwise stated. Water, purified to a resistivity of 18.2 MΩ/cm, was obtained from a Milli-Q water system (EMD Millipore, Billerica, MA) and sterilized by autoclaving before using it to prepare hydrogels.

3.2.2 Synthesis of peptide-amphiphiles

Protected, custom peptides were purchased from United Biosystems (Herndon, VA). PR_g peptide ($GGGSSSPHSRN(SG)_5RGDSP$), Collagen I peptide (GGGSSSGTPGPQGIAGQRGVV), bFGF peptide (GGGSSSYRSRKYSSWYVALKR), heparin-binding peptide (GGGSSSLRKKLGKA), and the E2 diluent peptide (GGGSSESE), were synthesized using standard Fmoc solid phase synthesis on peptide amide linker resin. The Fmoc protecting group was removed using a solution of 20% piperidine in dimethylformamide (DMF). A palmitic acid, C_{16}, tail was coupled to the N-terminus of the peptide with 4.5 molar equivalents of N,N,N′,N′-Tetramethyl-O-(1H-benzotriazol -1-yl)uronium hexafluorophosphate (HBTU), 4.5 molar equivalents of palmitic acid, and 6 molar equivalents of diisopropylethylamine in DMF for 4 h. The Kaiser test was used to verify complete coupling of the tails to the peptide amide. The resin beads were washed twice in DMF, dichloromethane, and methanol and dried overnight under vacuum. Peptide-amphiphiles were cleaved from resin in a cleavage cocktail of 90% trifluoroacetic acid (TFA), 5% thioanisole, 3% 1,2-ethandithiol, and 2% anisole for 2 h. The solution was collected and precipitated in 20X excess cold isopropyl ether. The precipitate was collected by centrifugation (10 min at 7,000 RCF), dried, redissolved in Milli-Q water and purified using reversed phase high performance liquid chromatography (HPLC) on an Agilent 1100 Series system with a Waters Xterra Prep MS C18 column, using a water/methanol gradient with 0.1% TFA for PR_g, Collagen I,

bFGF, and heparin-binding or 0.1% ammonium hydroxide for E2. The pure peptide-amphiphile product was analyzed with the Bruker BioTOF II to verify that the product had the expected mass. Peptide-amphiphiles were stored as lyophilized powder at -20 °C. Stock solutions of peptide-amphiphiles were prepared in Milli-Q water from the lyophilized peptide-amphiphiles and aliquots were stored at -20 °C to avoid freeze-thaw. All peptide-amphiphile gels in this study contained 5 mol % bioactive peptide (PR_g, collagen I, bFGF, or heparin-binding) and 95, 90, or 80 mol % E2.

3.2.3 Rheology

The mechanical properties of multifunctional peptide-amphiphile hydrogels without cells were characterized using an AR-G2 rheometer from TA Instruments. 2X concentrations of peptide-amphiphile solutions containing 5 mol % of (N) bioactive peptide-amphiphiles and (100 – 5N) mol % E2 were loaded onto the peltier plate and mixed with an equal volume of DMEM media supplemented with 10 mM $CaCl_2$. For example, a hydrogel with PR_g and bFGF had 5 mol % PR_g, 5 mol % bFGF and 90 mol % E2. Immediately after mixing, the 8 mm parallel plate was lowered to a gap of 500 μm and the peltier plate was heated to 37 °C. The gels were allowed to mature in a hydrated chamber for 2 h before frequency sweep measurements were made from 0.1 to 10 rad/s at 1% strain. Strain sweeps performed prior to frequency sweeps showed that 1% strain fell within the linear viscoelastic regime.

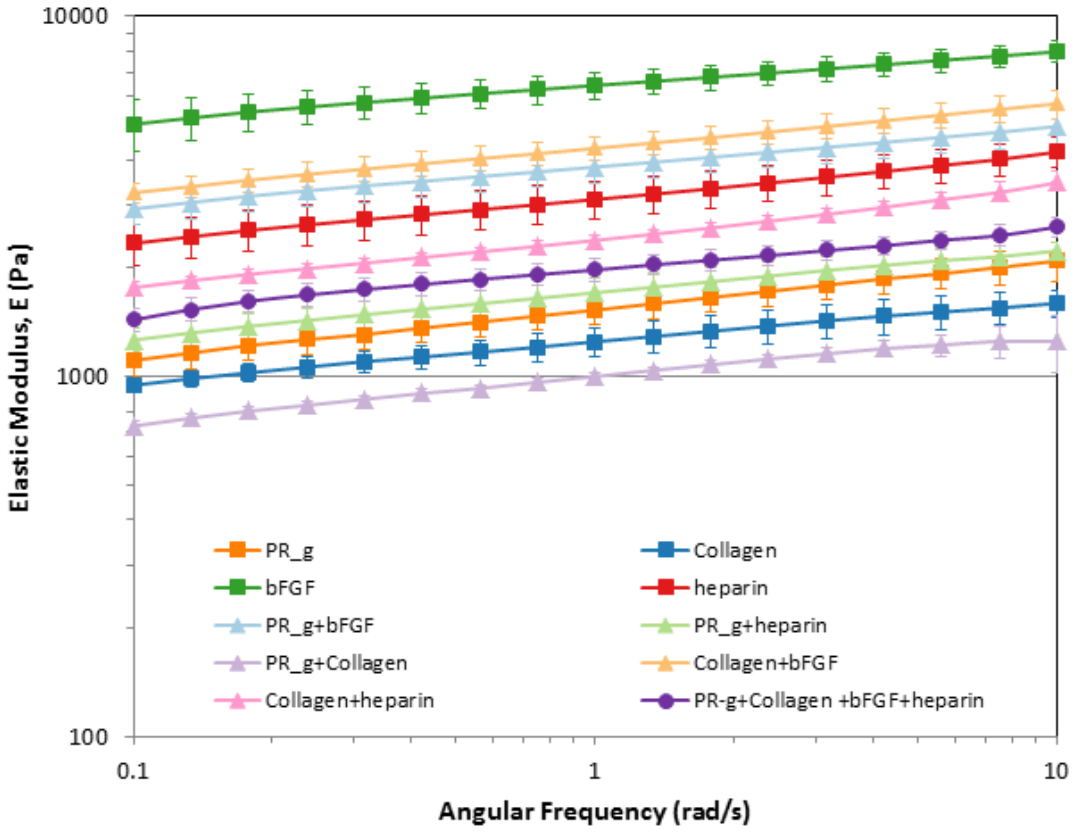

Figure 3.1: Rheology of 1.0 wt% bioactive peptide-amphiphiles mixed with E2 diluent peptide-amphiphiles. Each bioactive peptide is added at a 5 mol% concentration with 95, 90 or 80 mol % E2 diluent. Data are shown as mean ± standard error from three independent experiments (*n*=3).

3.3 Results and Discussion

The elastic modulus of 1.0 wt % multifunctional peptide-amphiphile hydrogels is shown in Figure 3.1, and ranges from 1000 Pa to 6500 Pa. For individual bioactive peptide-amphiphiles, 5 mol % in 95 mol % E2, the more positively charged the bioactive peptide-amphiphiles, the higher the hydrogel modulus. Hydrogels with pairs of bioactive peptide-amphiphiles containing the highly positively charged bFGF or heparin binding peptides

have a higher modulus than hydrogels with the PR-g or collagen I peptide alone and the PR_g + collagen I peptide pair. The hydrogel containing 5 mol % of each bioactive peptide-amphiphile has an intermediate modulus, indicating that both peptide sequence and E2 content affect the hydrogel modulus. While the increased number of parameters may be attractive for tuning the modulus of the hydrogel in the future, it makes studying the effect of the bioactive peptides difficult because the effect of the peptide sequence and hydrogel modulus cannot be deconvoluted. As a result, bioactive-peptides covalently immobilized on multiwell plates were investigated to evaluate the effect of the peptides in a simpler system.

3.4 Conclusions

Design of scaffolds which incorporate multiple bioactive peptide-amphiphiles can better reproduce the complex signaling of the native ECM in a tissue specific manner. However, because both peptide sequence and E2 content affect the hydrogel modulus, it is difficult to deconvolute the effect of the peptide sequence from the effect of the hydrogel modulus. As a result, a simplified, peptide-functionalized surface will be used to study the effects of the bioactive peptides.

Chapter 4 Effect of extracellular matrix protein- and growth factor-mimetic peptides on β-cell proliferation and insulin secretion

4.1 Summary

Covalently immobilized peptide mimetics of fibronectin, laminin, basic fibroblast growth factor, and glucagon-like peptide-1 and combinations thereof were evaluated using mouse insulinoma cells (MIN6), a pancreatic beta cell line. MIN6 cell proliferation on peptide-functionalized surfaces was significantly greater compared to blank surfaces (hydrolyzed maleimide with no peptides) and similar to tissue culture treated (TCT) plates. However, peptide-functionalized surfaces supported a three-dimensional (3D) morphology of MIN6 cells, similar to pseudoislets, while cells on TCT surfaces maintained a spread morphology. An increase in insulin secretion from MIN6 cells on peptide-functionalized surfaces was also observed compared to TCT plates, though there were no statistically significant differences between individual peptides and peptide combinations. To investigate if peptide functionalization can have an effect on 3D cell entrapment, poly(ethylene glycol) dimethacrylate ($PEGDM_{10K}$) hydrogels were functionalized with the laminin-mimetic IKVAV peptide as a proof of concept. Hydrogels with the IKVAV peptide supported significantly greater proliferation and insulin production of entrapped MIN6 cells compared to non-functionalized $PEGDM_{10K}$

hydrogels supporting the hypothesis that peptide-functionalization of the $PEGDM_{10K}$ hydrogel can promote survival and function of entrapped β-cells.

4.2 Introduction

Insulin producing cells are of great interest in the search for treatments of type 1 diabetes (T1D). One of the most promising treatments for T1D is the transplantation of pancreatic islets from a healthy donor. However, issues with this treatment include the limited availability of donor islets, loss of islet viability, and poor engraftment and survival in the recipient.[134–136] Many studies have shown the importance of the islet-extracellular matrix (ECM) relationship, which is disrupted upon islet isolation.[137,138] The use of relevant ECM proteins, including collagen I, collagen IV, fibronectin, and laminin has been shown to support increased viability, proliferation, and insulin secretion in β-cells and islets.[137–142] Natural ECMs, such as decellularized tissue, have been shown to improve β-cell and islet viability and function more than ECM proteins alone.[143–145] This improvement is likely due to the increased complexity and additional signaling factors present, but these scaffolds are not defined and can have batch to batch variability similar to ECM proteins. Additionally, growth factors have been shown to play an important role in β-cell and islet function and survival. The ubiquitous, basic fibroblast growth factor (bFGF) has been shown to have mitogenic and immunoprotective effects on β-cells and has been shown to increase viability of transplanted islets, likely as a result of increased

vascularization.[146–148] Glucagon-like peptide-1 (GLP-1) has been shown to provide immunoprotection from inflammatory cytokines in addition to stimulating β-cell proliferation.[149–151] Other growth factors, including hepatocyte growth factor (HGF), parathyroid hormone-related protein (PTHrP), as well as insulin and insulin-like growth factors (IGFs) have been shown to increase β-cell proliferation.[152]

While the use of full proteins and growth factors has been shown to be effective for β-cell culture, they can be expensive to produce and purify, there can be batch to batch variability, and control over their orientation when functionalizing surfaces and scaffolds can be limited.[153,154] These limitations have driven the design of many peptide mimetics, which allow for increased epitope density, increased control over epitope orientation, and increases in proteolytic stability.[155] Peptide mimetics of ECM components have also been shown to be effective for supporting islet and β-cell viability and insulin secretion.[156–161]

High performing peptide mimetics of fibronectin, laminin, bFGF, and GLP-1 have been selected for investigation in the present study. The fibronectin-mimetic PR_g peptide contains the RGD cell binding site and the PHSRN synergy site, separated by a linker which reproduces the distance and the hydrophobicity/hydrophilicity between these domains in the native protein.[42,53,54] Porcine islets cultured in medium supplemented with this fibronectin-mimetic peptide demonstrated increased levels of ECM fibronectin secretion compared to normal culture conditions.[162] The PR_g peptide has been shown to

support increased cell adhesion, proliferation, and ECM deposition in a variety of cell types.[61,163] The laminin-mimetic IKVAV peptide has been shown to promote β-cell adhesion and viability[161] in addition to stimulating axon growth in neural cells.[164,165] Growth factor-mimetics of bFGF and GLP-1 have been shown to produce similar cell responses and signaling as their full protein counterparts.[126,127,166] Additionally, the immobilization of growth factors has been shown to improve their stability, persistence, and mitogenic effect.[167,168] While adhesive mimetic peptides and growth factor mimetic peptides have been shown to be effective individually, little has been done to evaluate the potential of combining these two classes of peptide mimetics. The present study uses covalently immobilized peptide mimetics of fibronectin, laminin, bFGF, and GLP-1 on surfaces to investigate the potential synergy or benefit of peptides and combinations of peptide mimetics of two classes of proteins, adhesion proteins and growth factors, to support β-cell proliferation and insulin secretion. While it is beyond the scope of this study to carefully investigate peptide-mimetics in 3D hydrogels, poly (ethylene glycol) dimethacrylate ($PEGDM_{10K}$) hydrogels were functionalized with the laminin-mimetic IKVAV peptide and used to investigate the effect of peptide-functionalization on cell proliferation and insulin production after cell entrapment. The IKVAV peptide was selected due to its prevalence in the literature of β-cells.

4.3 Experimental methods

4.3.1 Materials

All chemicals were purchased from Thermo Fisher Scientific unless otherwise stated. Custom peptides were purchased from United Biosystems (Herndon, VA) and maleimide functionalized Sulfhydryl-BIND 96 well plates were purchased from Sigma-Aldrich. MIN6 cells were purchased from AddexBio (San Diego, CA) and Dulbecco's modified Eagle's medium (DMEM) was purchased from Life Technologies (Grand Island, NY). The insulin ELISAs were purchased from Mercodia Inc. (Uppsala, Sweden). PEG_{10K} (MW = 10,000), methacrylic anhydride, and 2-hydroxy-2-methylpropiophenone were purchased from Sigma-Aldrich. Acrylate-$PEG_{3.4K}$-Maleimide (MW 3,400) was purchased from Laysan Bio (Arab, AL).

4.3.2 MIN6 culture

The MIN6 murine pancreatic β-cell line was cultured in DMEM supplemented with 10 % fetal bovine serum (FBS), 1% penicillin-streptomycin, and 50 μM β-mercaptoethanol at 37 °C with 5% CO_2. Media was changed every 2 to 3 days until cells reached confluency and were passaged. Cells were used between passages 17 and 27 for this study.

4.3.3 Surface preparation

Crude cysteine-peptides were purchased from United Biosystems (Herndon, VA): PR_g, C-GGGSSPHSRN$(SG)_5$RGDSP; laminin, C-GGGSSIKVAV; GLP-1, C-GGGSSHSEGTFTSD; and bFGF, C-GGGSSYRSRKYSSWYVALKR. Crude peptides were purified using reverse-phase high-performance liquid chromatography (HPLC) on an Agilent 1100 series system with a Waters Xterra Prep MS C18 column using a water/methanol gradient with 0.1% trifluoroacetic acid (TFA). Purified cysteine-peptides were dissolved in 5 mM tris(2-carboxyethl) phosphine (TCEP) in phosphate buffered saline (PBS) and allowed to sit for 10 min to reduce disulfide bonds. 100 μL of each 3 μM peptide solution was added to Sulfhydryl-BIND plates and allowed to react overnight. Before cell seeding, peptide solutions were removed and surfaces were washed with 0.4% bovine serum albumin (BSA) in PBS 3 times for 5 min. For surface studies, MIN6 cells were seeded at a density of 25,000 cells per well. Media on surfaces was changed every 3 days.

4.3.4 Cell viability and proliferation assays

Cell proliferation was evaluated using the Cell Titer GLO assay (Promega, Madison, WI) according to manufacturer's instructions. Cell viability was also evaluated using the Live/Dead assay according to manufacturer's instructions. Fluorescence images were acquired using the GFP light cube (excitation 470/22 nm, emission 510/542 nm) and the

Texas Red light cube (excitation 585/ 529 nm, emission 624/640 nm). Surfaces were imaged using the EVOS®fl integrated light microscope from the Advanced Microscopy Group (Bothell, WA).

4.3.5 Glucose-stimulated insulin secretion

Surfaces and hydrogels containing encapsulated MIN6 β-cells were rinsed and incubated in Krebs buffer (25 mM HEPES, 115 mM NaCl, 24 mM $NaHCO_3$, 5 mM KCl, 2.5 mM $CaCl_2$-H_2O, 1 mM $MgCl_2$-$6H_2O$, 0.1% BSA, pH 7.4) supplemented with 1.1 mM glucose at 37 ℃ for 45 min. Media was then replaced with Krebs buffer supplemented with 16.7 mM glucose and incubated for 1 h at 37 °C.[169] Following incubation, media was collected to measure insulin concentration via ELISA.

4.3.6 PEGDM synthesis and characterization

$PEGDM_{10K}$ was synthesized from linear PEG_{10K} with methacrylic anhydride as previously described.[170] Briefly, 1 g PEG_{10K} and a 10-fold molar excess of methacrylic anhydride were mixed in a capped borosilicate glass vial. The mixture was placed in a microwave oven (RCA, 900 W) for 10 min in 1 min intervals with 1 min of cooling in between. The mixture was then dissolved in a small volume of methanol and $PEGDM_{10K}$ was precipitated in an excess of ethyl ether.[170] The $PEGDM_{10K}$ was collected using a sintered glass filter, dried in the hood for several hours, ground with a mortar and pestle, and dried overnight under vacuum. ^1H NMR was used to verify the conversion of PEG_{10K}

to $PEGDM_{10K}$. ^{1}H NMR spectra were recorded in deuterated chloroform ($CDCl_3$) on a Varian INOVA-300 spectrometer at room temperature.

4.3.7 Acrylate-PEG-peptide synthesis and characterization

Purified cysteine-peptide was dissolved in 25 mM TCEP in PBS and allowed to sit for 10 min to reduce disulfide bonds. Reduced cysteine-peptide and acrylate-$PEG_{3.4K}$-maleimide were re-acted in 1.2:1 molar ratios at room temperature overnight, protected from light. The acrylate-$PEG_{3.4K}$-peptide was dialyzed overnight in DI water to remove unreacted peptide and the final product was lyophilized, protected from light. Acrylate-$PEG_{3.4K}$-maleimide, cysteine-peptide, and acrylate-$PEG_{3.4K}$-peptide were characterized with ^{1}H NMR in D_2O on a Varian INOVA-300 spectrometer at room temperature.

4.3.8 Hydrogel preparation

For 3D cell entrapment, MIN6 cells were suspended in $PEGDM_{10K}$ solutions containing 0 or 20 μM acrylate-$PEG_{3.4K}$-IKVAV at a concentration of $2x10^7$ cells/mL. 40 μL of cell-PEG solutions were pipetted into molds created from 1 mL syringes and exposed to 365 nm UV light (B-100AP, UVP, Upland, CA), ~11 mW/cm^2, for 7 min. Gels were washed in PBS to remove non-crosslinking polymer and unentrapped cells, and then transferred to media in multiwell plates. Media on hydrogels was replenished every 3 days.

4.3.9 Rheology

Hydrogels were formed from a 10 wt% solution of PEGDM in Hanks Buffered Salt Solution (HBSS) with 0.025% v/v 2-hydroxy-2-methylpropiophenone ex-posed to 365 nm UV light at an intensity of ~11 mW/cm2 for 7 minutes. Hydrogels were formed in a 7.9 mm diameter mold and allowed to swell in PBS. The mechanical properties of the hydrogels were characterized using an AR-G2 rheometer from TA instruments (New Castle, DE). The peltier plate, heated to 25°C, was used with an 8 mm parallel plate. Strain sweeps were performed to select a %strain within the linear viscoelastic regime. Frequency sweep measurements were made from 100 to 0.1 rad/s at 2% strain. Hydrogels with 0, 10, 20, and 30 μM concentrations of acrylate-$PEG_{3.4K}$-IKVAV peptide were measured.

4.3.10 Statistical analysis

All data are reported as mean ± SEM from n≥3 independent experiments. Differences among groups were assessed using ANOVA followed by Tukey's HSD.

4.4 Results and discussion

4.4.1 Cell viability and proliferation

Peptides were immobilized on surfaces using maleimide chemistry to allow for controlled orientation of peptide mimetics. Control surfaces included the hydrolyzed-maleimide

(blank) surface and the tissue culture treated (TCT) surface. The TCT control was included because these surfaces are ubiquitously used for cell culture and can be considered the standard in the field. The number of cells on each surface significantly increased over time for all surfaces as shown in Figure 4.1, (*p*-values from ANOVA and Tukey's HSD analysis of MIN6 proliferation can be found in Tables 4.1 and 4.2. At the day 1 (d1) time point, the TCT surface had a statistically significantly higher number of adherent cells compared to all other surfaces. This is unsurprising given that TCT plastic is designed to facilitate adsorption of serum proteins and rapid cell adhesion. By day 4 (d4), the blank control surface has statistically significantly fewer cells than all of the peptide surfaces and the TCT surface. All of the peptide surfaces support cell proliferation at least as well as the TCT surface, with PR_g, IKVAV, and bFGF surfaces supporting greater proliferation at d4 compared to the TCT surface. By day 7 (d7), the TCT surface only supports significantly more cells compared to the blank, IKVAV + PR_g, and the all peptide surfaces. All individual peptides and all peptide pairs other than IKVAV + PR_g supported significantly more proliferation compared to the blank surfaces and support at least as much proliferation as the TCT surfaces. These results indicated that there was no synergistic benefit on cell proliferation from combining adhesive peptides or adhesive and growth factor peptide mimetics. Even though there are no previous reports on the effect of combining adhesion proteins with growth factors, others have reported a similar lack of synergistic response of β-cells and islets with combinations of collagen and laminin proteins.[141,142]

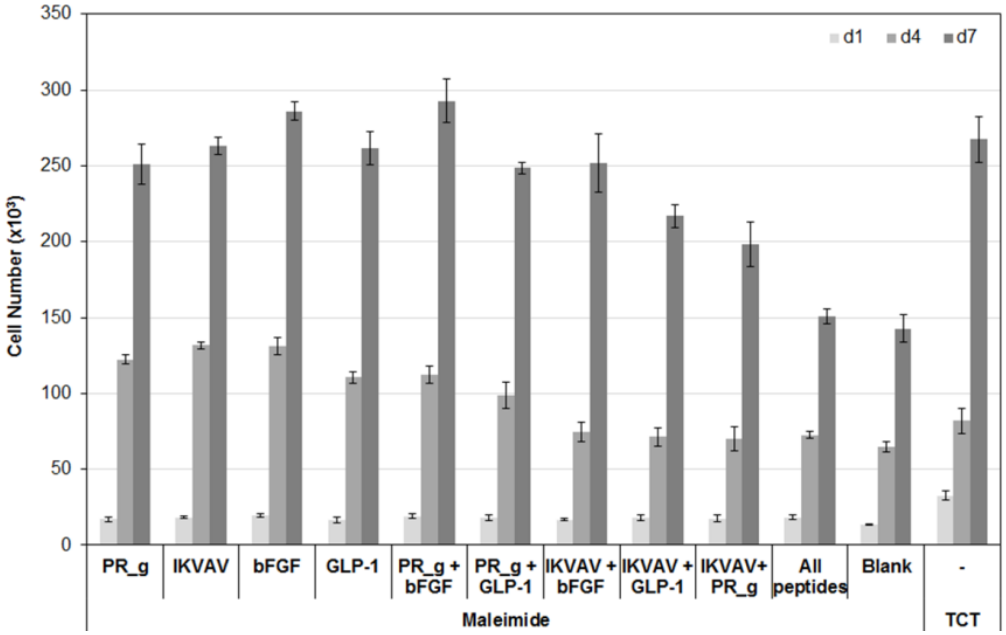

Figure 4.1: MIN6 cell proliferation on peptide-functionalized surfaces and controls (TCT and blank plates) over time. Data represent mean ± SEM from n≥4 independent experiments performed in quadruplicate. Tables of p-values are located in Tables 4.1 and 4.2.

Phase images shown in Figure 4.2 are consistent with the quantification of cell proliferation. Additionally, the MIN6 cells are shown to have a flatter, more spread morphology on the TCT surfaces compared to the peptide surfaces. MIN6 cells on the peptide and blank surfaces developed a more 3D morphology over time, which may be more consistent with the morphology observed in islets and pseudoislets. The presence of 3D cell aggregates was verified by changing the focal plane and representative images are shown in the supporting information, Figure 4.3, for the GLP-1 and IKVAV + bFGF surfaces. The absence of cell aggregates on TCT surfaces can also be seen in Figure 4.3. The MIN6 cells on the IKVAV + PR_g surface and the surface with all peptides, which

supported less proliferation, also appear to have a less 3D morphology than MIN6 cells on other peptide surfaces. MIN6 cells on the blank surface also developed a 3D morphology, although the size and number of aggregates or pseudoislets is smaller than those on other peptide surfaces. The morphology observed on the blank surfaces Live/dead staining (Figure 4.4) shows very little cell death, indicating that the majority of the cells in the 3D aggregates or pseudoislets are viable.

Table 4.1: p-values from the ANOVA and Tukey's HSD analysis of MIN6 cell proliferation on peptide-functionalized surfaces and controls at d1, d4, and d7 as shown in Figure 4.1.

d1	PR_g	IKVAV	bFGF	GLP-1	PR_g + bFGF	PR_g + GLP-1	IKVAV + bFGF	IKVAV + GLP-1	IKVAV+ PR_g	All peptide	blank	TCT
PR_g		> 0.05	> 0.05	> 0.05	> 0.05	> 0.05	> 0.05	> 0.05	> 0.05	> 0.05	> 0.05	< 0.001
IKVAV			> 0.05	> 0.05	> 0.05	> 0.05	> 0.05	> 0.05	> 0.05	> 0.05	> 0.05	< 0.001
bFGF				> 0.05	> 0.05	> 0.05	> 0.05	> 0.05	> 0.05	> 0.05	> 0.05	< 0.001
GLP-1					> 0.05	> 0.05	> 0.05	> 0.05	> 0.05	> 0.05	> 0.05	< 0.001
PR_g + bFGF						> 0.05	> 0.05	> 0.05	> 0.05	> 0.05	> 0.05	< 0.001
PR_g + GLP-1							> 0.05	> 0.05	> 0.05	> 0.05	> 0.05	< 0.001
IKVAV + bFGF								> 0.05	> 0.05	> 0.05	> 0.05	< 0.001
IKVAV + GLP-1									> 0.05	> 0.05	> 0.05	< 0.001
IKVAV+ PR_g										> 0.05	> 0.05	< 0.001
All peptide											> 0.05	< 0.001
blank												< 0.001
TCT												

d4	PR_g	IKVAV	bFGF	GLP-1	PR_g + bFGF	PR_g + GLP-1	IKVAV + bFGF	IKVAV + GLP-1	IKVAV+ PR_g	All peptide	blank	TCT
PR_g		> 0.05	> 0.05	> 0.05	> 0.05	> 0.05	< 0.001	< 0.001	< 0.001	> 0.05	< 0.001	< 0.01
IKVAV			> 0.05	> 0.05	> 0.05	< 0.05	< 0.001	< 0.001	< 0.001	< 0.001	< 0.001	< 0.001
bFGF				> 0.05	> 0.05	< 0.05	< 0.001	< 0.001	< 0.001	< 0.001	< 0.001	< 0.001
GLP-1					> 0.05	> 0.05	< 0.05	< 0.01	< 0.01	< 0.01	< 0.001	> 0.05
PR_g + bFGF						> 0.05	< 0.01	< 0.01	< 0.01	< 0.01	< 0.001	> 0.05
PR_g + GLP-1							> 0.05	> 0.05	> 0.05	> 0.05	< 0.05	> 0.05
IKVAV + bFGF								> 0.05	> 0.05	> 0.05	< 0.05	> 0.05
IKVAV + GLP-1									> 0.05	> 0.05	< 0.05	> 0.05
IKVAV+ PR_g										> 0.05	< 0.05	> 0.05
All peptide											< 0.05	> 0.05
blank												> 0.05
TCT												

d7	PR_g	IKVAV	bFGF	GLP-1	PR_g + bFGF	PR_g + GLP-1	IKVAV + bFGF	IKVAV + GLP-1	IKVAV+ PR_g	All peptide	blank	TCT
PR_g		> 0.05	< 0.01	> 0.05	> 0.05	> 0.05	> 0.05	> 0.05	> 0.05	< 0.0001	< 0.0001	> 0.05
IKVAV			> 0.05	> 0.05	> 0.05	> 0.05	> 0.05	> 0.05	< 0.05	< 0.0001	< 0.0001	> 0.05
bFGF				> 0.05	> 0.05	> 0.05	> 0.05	< 0.01	< 0.01	< 0.0001	< 0.0001	> 0.05
GLP-1					> 0.05	> 0.05	> 0.05	> 0.05	< 0.05	< 0.0001	< 0.0001	> 0.05
PR_g + bFGF						> 0.05	> 0.05	> 0.05	> 0.05	< 0.0001	< 0.0001	> 0.05
PR_g + GLP-1							> 0.05	> 0.05	> 0.05	< 0.0001	< 0.0001	> 0.05
IKVAV + bFGF								> 0.05	< 0.0001	< 0.0001	< 0.0001	> 0.05
IKVAV + GLP-1									> 0.05	< 0.05	< 0.01	> 0.05
IKVAV+ PR_g										> 0.05	> 0.05	< 0.01
All peptide											> 0.05	< 0.0001
blank												< 0.0001
TCT												

Table 4.2: p-values from the ANOVA and Tukey's HSD analysis of MIN6 cell proliferation on peptide-functionalized surfaces and controls over time, shown in Figure 4.1.

PR_g	d1	d4	d7	PR_g + bFGF	d1	d4	d7	IKVAV + PR_g	d1	d4	d7
d1		< 0.001	< 0.001	d1		< 0.001	< 0.001	d1		< 0.01	< 0.001
d4			< 0.001	d4			< 0.001	d4			< 0.001
d7				d7				d7			
IKVAV	**d1**	**d4**	**d7**	**PR_g + GLP-1**	**d1**	**d4**	**d7**	**All peptide**	**d1**	**d4**	**d7**
d1		< 0.001	< 0.001	d1		< 0.001	< 0.001	d1		< 0.001	< 0.001
d4			< 0.001	d4			< 0.001	d4			< 0.001
d7				d7				d7			
bFGF	**d1**	**d4**	**d7**	**IKVAV + bFGF**	**d1**	**d4**	**d7**	**Blank**	**d1**	**d4**	**d7**
d1		< 0.001	< 0.001	d1		< 0.01	< 0.001	d1		< 0.001	< 0.001
d4			< 0.001	d4			< 0.001	d4			< 0.001
d7				d7				d7			
GLP-1	**d1**	**d4**	**d7**	**IKVAV + GLP-1**	**d1**	**d4**	**d7**	**TCT**	**d1**	**d4**	**d7**
d1		< 0.001	< 0.001	d1		< 0.001	< 0.001	d1		< 0.05	< 0.001
d4			< 0.001	d4			< 0.001	d4			< 0.001
d7				d7				d7			

4.4.2 Insulin secretion

The insulin secreted by MIN6 cells on peptide-functionalized surfaces was quantified via ELISA and results are shown in Figure 4.4 (*p*-values from ANOVA and Tukey's HSD analysis of insulin secretion from MIN6 cells can be found in Tables 4.3 and 4.4. While the amount of insulin secreted significantly increased over time on all surfaces, the peptide functionalized surfaces supported significantly higher insulin secretion compared to TCT as early as d4. Only the PR_g peptide surface supported insulin secretion that was not statistically different from the insulin secretion on TCT surfaces at d4. MIN6 cells on GLP-1, IKVAV + bFGF, and the IKVAV + GLP-1 surfaces secreted significantly higher amounts of insulin compared to MIN6 cells on the blank surface at d4 as well. By d7, MIN6 cells on every peptide surface secreted significantly more insulin than those on

TCT surfaces and cells on PR_g, bFGF, IKVAV + bFGF, and IKVAV + GLP-1 surfaces secrete significantly more insulin than cells on blank surfaces. These trends indicate that the presence of peptides leads to higher insulin secretion in addition to increasing proliferation. The lack of differences between the insulin secreted from MIN6 cells on different peptide surfaces suggests that the 3D morphology of the cells and the resulting cell-cell signaling may play a more important role in β-cell function than the type of peptide mimetic used. The cell-cell signaling molecule E-cadherin, for example, has been shown to play a critical role in the secretory function of β-cells. Decreases in insulin secretion and cell-cell tight junctions as well as loosening of β-cell pseudoislet morphology when E-cadherin signaling was blocked.[171,172] β-cell viability in non-functionalized PEG scaffolds was dependent on cell seeding density, and long term viability was only achieved with cell densities greater than $1x10^7$ cells/mL. Functionalizing PEG scaffolds with fusion proteins of cell-cell signaling molecules such as the ephrin A ligand and EphA receptor recovered cell viability at significantly lower cell seeding densities, again highlighting the importance of cell-cell signaling in β-cell viability and function.[173]

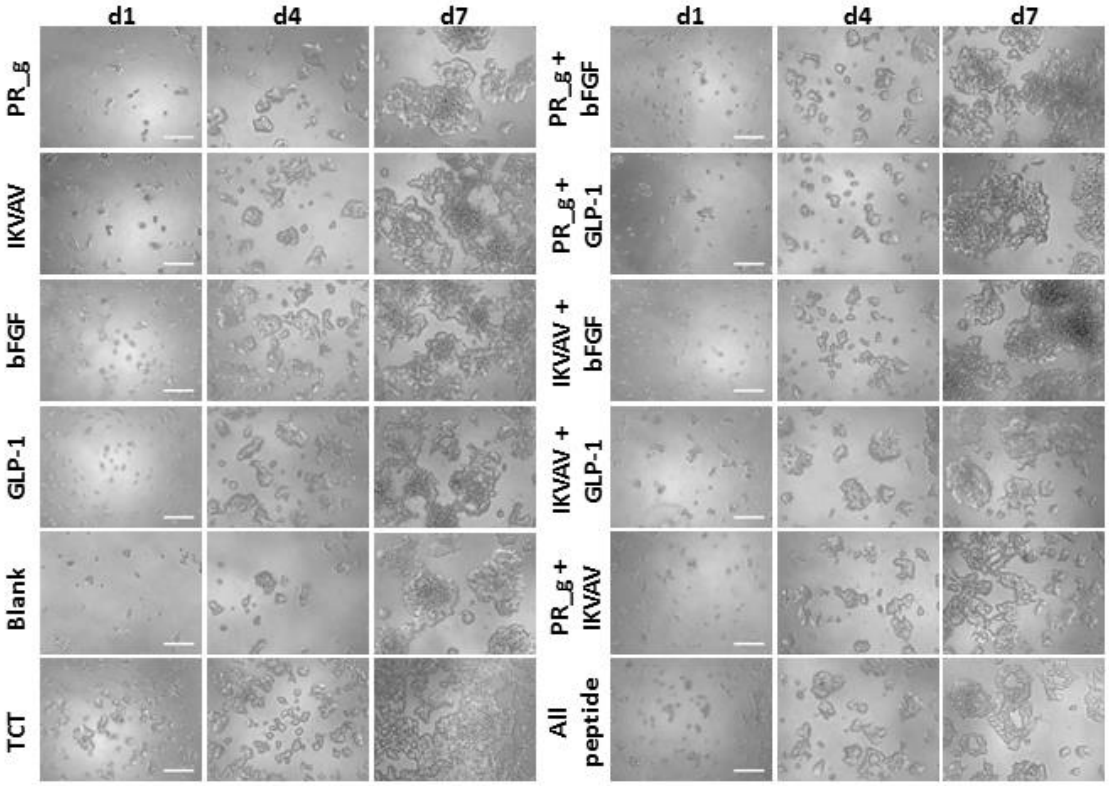

Figure 4.2: Phase contrast images of MIN6 cells on peptide-functionalized surfaces and controls over time. Scale bars are 200 μm.

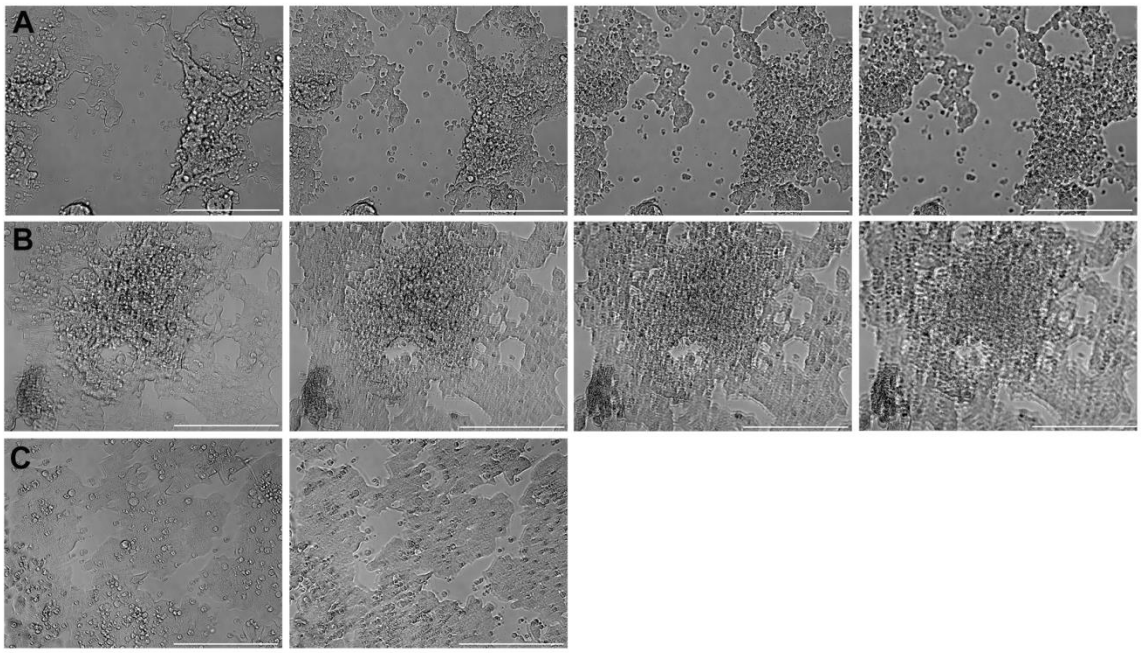

Figure 4.3: Phase contrast images of MIN6 cells on (A) GLP-1, (B) IKVAV + bFGF and (C) TCT surfaces after 7 days of culture. The presence of 3D cell aggregates on the peptide surfaces (A, B) and absence of 3D cell aggregates on TCT surfaces (C) can be seen as the focal plane is raised from the surface (left images) to the top layer (right images). Scale bars are 200 μm.

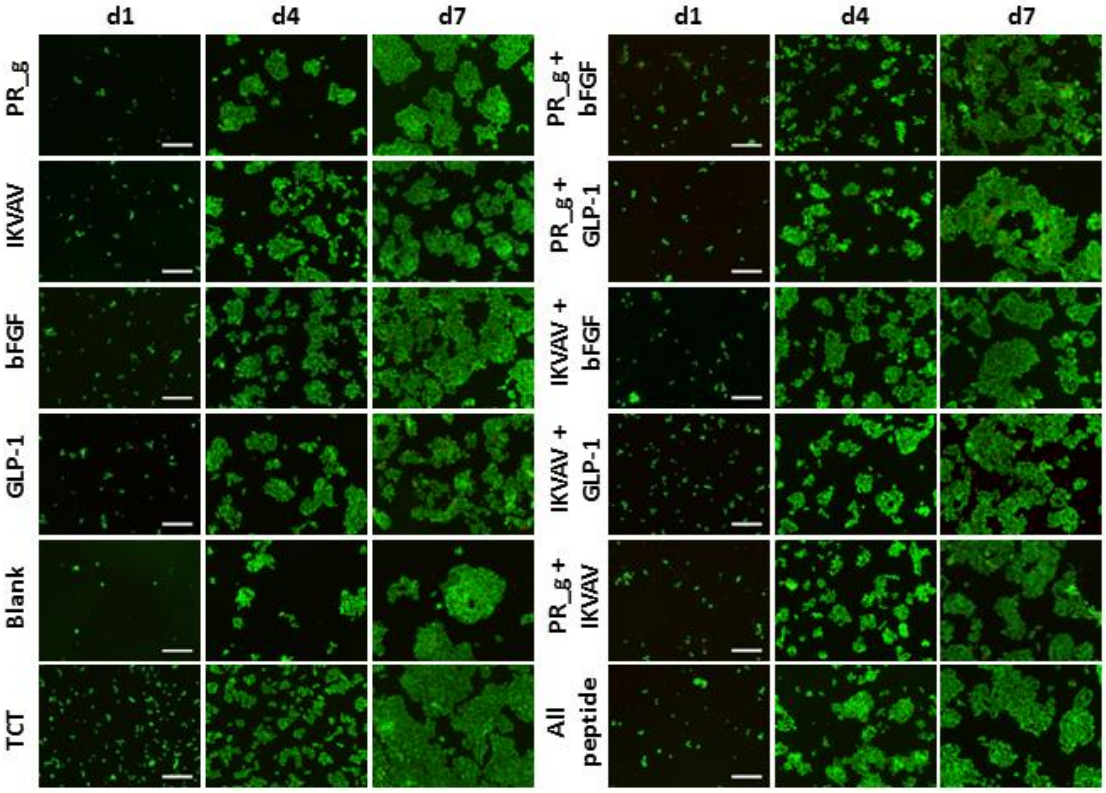

Figure 4.4: Live/Dead stain of MIN6 cells on peptide-functionalized surfaces and controls over time. Green shows live cells, red indicates membrane compromised cells. Scale bars are 200 μm.

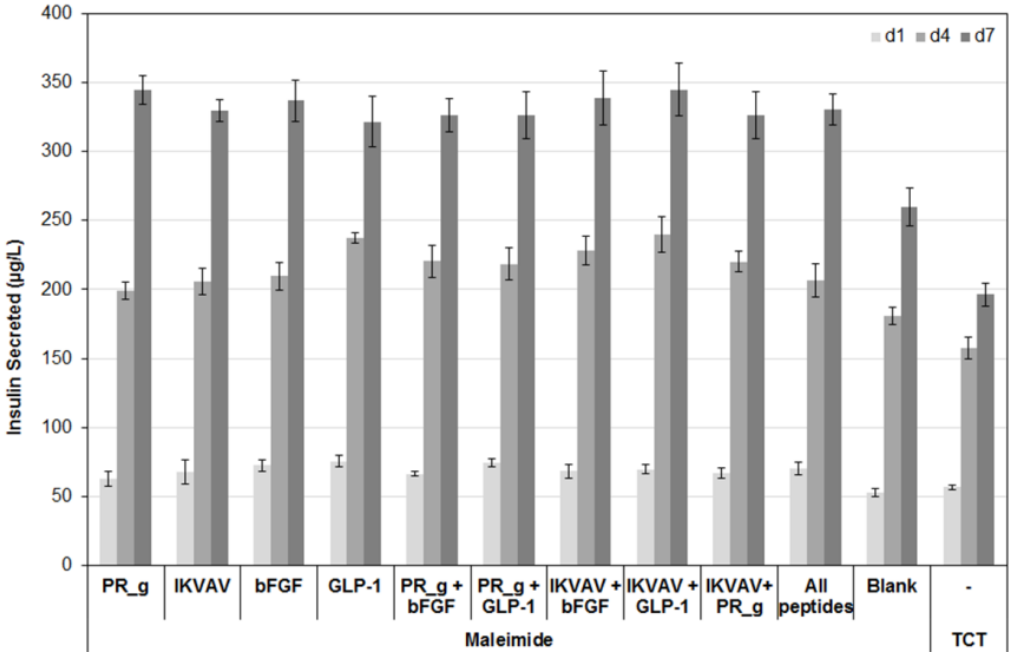

Figure 4.5: Insulin secreted from MIN6 cells on peptide-functionalized surfaces and controls over time. Data represent mean ± SEM from $n \geq 3$ independent experiments performed in triplicate. Tables of p-values are reported in Table 4.3 and 4.4.

Table 4.3: p-values from the ANOVA and Tukey's HSD analysis of MIN6 insulin secretion on peptide-functionalized and control surfaces at d1, d4, and d7, shown in Figure 4.5.

d1	PR_g	IKVAV	bFGF	GLP-1	PR_g + bFGF	PR_g + GLP-1	IKVAV + bFGF	IKVAV + GLP-1	IKVAV+ PR_g	All peptide	Blank	TCT
PR_g		> 0.05	> 0.05	> 0.05	> 0.05	> 0.05	> 0.05	> 0.05	> 0.05	> 0.05	> 0.05	> 0.05
IKVAV			> 0.05	> 0.05	> 0.05	> 0.05	> 0.05	> 0.05	> 0.05	> 0.05	> 0.05	> 0.05
bFGF				> 0.05	> 0.05	> 0.05	> 0.05	> 0.05	> 0.05	> 0.05	< 0.05	< 0.05
GLP-1					> 0.05	> 0.05	> 0.05	> 0.05	> 0.05	> 0.05	> 0.05	> 0.05
PR_g + bFGF						> 0.05	> 0.05	> 0.05	> 0.05	> 0.05	> 0.05	> 0.05
PR_g + GLP-1							> 0.05	> 0.05	> 0.05	> 0.05	> 0.05	> 0.05
IKVAV + bFGF								> 0.05	> 0.05	> 0.05	> 0.05	> 0.05
IKVAV + GLP-1									> 0.05	> 0.05	> 0.05	> 0.05
IKVAV+ PR_g										> 0.05	> 0.05	> 0.05
All peptide											> 0.05	> 0.05
blank												> 0.05
TCT												

d4	PR_g	IKVAV	bFGF	GLP-1	PR_g + bFGF	PR_g + GLP-1	IKVAV + bFGF	IKVAV + GLP-1	IKVAV+ PR_g	All peptide	blank	TCT
PR_g		> 0.05	> 0.05	> 0.05	> 0.05	> 0.05	> 0.05	> 0.05	> 0.05	> 0.05	> 0.05	> 0.05
IKVAV			> 0.05	> 0.05	> 0.05	> 0.05	> 0.05	> 0.05	> 0.05	> 0.05	> 0.05	< 0.05
bFGF				> 0.05	> 0.05	> 0.05	> 0.05	> 0.05	> 0.05	> 0.05	> 0.05	< 0.05
GLP-1					> 0.05	> 0.05	> 0.05	> 0.05	> 0.05	> 0.05	< 0.05	< 0.01
PR_g + bFGF						> 0.05	> 0.05	> 0.05	> 0.05	> 0.05	> 0.05	< 0.01
PR_g + GLP-1							> 0.05	> 0.05	> 0.05	> 0.05	> 0.05	< 0.01
IKVAV + bFGF								> 0.05	> 0.05	> 0.05	< 0.05	< 0.01
IKVAV + GLP-1									> 0.05	> 0.05	< 0.01	< 0.01
IKVAV+ PR_g										> 0.05	> 0.05	< 0.01
All peptide											> 0.05	< 0.05
blank												> 0.05
TCT												

d7	PR_g	IKVAV	bFGF	GLP-1	PR_g + bFGF	PR_g + GLP-1	IKVAV + bFGF	IKVAV + GLP-1	IKVAV+ PR_g	All peptide	blank	TCT
PR_g		> 0.05	> 0.05	> 0.05	> 0.05	> 0.05	> 0.05	> 0.05	> 0.05	> 0.05	< 0.05	< 0.001
IKVAV			> 0.05	> 0.05	> 0.05	> 0.05	> 0.05	> 0.05	> 0.05	> 0.05	> 0.05	< 0.001
bFGF				> 0.05	> 0.05	> 0.05	> 0.05	> 0.05	> 0.05	> 0.05	< 0.05	< 0.001
GLP-1					> 0.05	> 0.05	> 0.05	> 0.05	> 0.05	> 0.05	> 0.05	< 0.001
PR_g + bFGF						> 0.05	> 0.05	> 0.05	> 0.05	> 0.05	> 0.05	< 0.001
PR_g + GLP-1							> 0.05	> 0.05	> 0.05	> 0.05	> 0.05	< 0.001
IKVAV + bFGF								> 0.05	> 0.05	> 0.05	< 0.05	< 0.001
IKVAV + GLP-1									> 0.05	> 0.05	< 0.05	< 0.001
IKVAV+ PR_g										> 0.05	> 0.05	< 0.001
All peptide											> 0.05	< 0.001
blank												> 0.05
TCT												

Table 4.4: p-values from the ANOVA and Tukey's HSD analysis of MIN6 insulin secretion of peptide-functionalized surfaces and controls over time, shown in Figure 4.5.

PR_g	d1	d4	d7	PR_g + bFGF	d1	d4	d7	IKVAV + PR_g	d1	d4	d7
d1		< 0.001	< 0.001	d1		< 0.001	< 0.001	d1		< 0.001	< 0.001
d4			< 0.001	d4			< 0.001	d4			< 0.001
d7				d7				d7			
IKVAV	**d1**	**d4**	**d7**	**PR_g + GLP-1**	**d1**	**d4**	**d7**	**All peptide**	**d1**	**d4**	**d7**
d1		< 0.001	< 0.001	d1		< 0.001	< 0.001	d1		< 0.001	< 0.001
d4			< 0.001	d4			< 0.001	d4			< 0.001
d7				d7				d7			
bFGF	**d1**	**d4**	**d7**	**IKVAV + bFGF**	**d1**	**d4**	**d7**	**Blank**	**d1**	**d4**	**d7**
d1		< 0.001	< 0.001	d1		< 0.001	< 0.001	d1		< 0.001	< 0.001
d4			< 0.001	d4			< 0.001	d4			< 0.001
d7				d7				d7			
GLP-1	**d1**	**d4**	**d7**	**IKVAV + GLP-1**	**d1**	**d4**	**d7**	**TCT**	**d1**	**d4**	**d7**
d1		< 0.001	< 0.001	d1		< 0.001	< 0.001	d1		< 0.001	< 0.001
d4			< 0.01	d4			< 0.001	d4			< 0.01
d7				d7				d7			

4.4.3 Hydrogel rheology

Results from the culture of MIN6 cells on different surfaces showed that the presence of peptides was favorable for cell proliferation and insulin secretion, however the peptide sequence did not have a significant effect overall. As a proof of concept that peptide-functionalized hydrogels may also influence cell proliferation and insulin secretion, $PEGDM_{10K}$ hydrogels covalently functionalized with the IKVAV peptide were characterized. The IKVAV peptide was selected due to its prevalence in the literature of β-cells. The synthesis of $PEGDM_{10K}$ and acrylate-$PEG_{3.4K}$-peptide were verified using ^{1}H NMR and are reported in Figure 4.6 and Figure 4.7. To ensure that the observed cell

responses are due to peptide bioactivity and not differences in mechanical properties of peptide-functionalized hydrogels rheological measurements of 10 wt% $PEGDM_{10K}$ hydrogels containing 0, 10, 20, and 30 μM acrylate-$PEG_{3.4K}$-IKVAV were evaluated (Figure 4.8). The modulus of 10 wt% $PEGDM_{10K}$ gels with 0 μM acrylate-PEG-peptide was 1262 ± 17 Pa. Mouse pancreatic tissue has been reported to have a modulus of 1210 ± 77 Pa, so 10 wt% $PEGDM_{10K}$ hydrogels are appropriate for the culture of β-cells.[26] The moduli of 10 wt% $PEGDM_{10K}$ hydrogels containing 10 μM and 20 μM acrylate-$PEG_{3.4K}$-IKVAV were 1244 ± 35 Pa and 1170 ± 20 Pa respectively and there was no statistical significance from the modulus of the 0 μM hydrogels. Hydrogels containing 30 μM acrylate-$PEG_{3.4K}$-IKVAV had a modulus of 1045 ± 15 Pa, and the difference to the modulus of the 0 μM hydrogels was statistically significant, As a result, all cell evaluations were done using 20 μM acryl-PEG-peptide in order to present the highest peptide concentration without changing the modulus of the hydrogel. The concentration of 20 μM acrylate-PEG3.4K-IKVAV is sufficient to elicit cell responses as immobilized transforming growth factor-β (TGF-β) concentrations as low as 40 pM have been shown to increase production of ECM proteins in vascular smooth muscle cells and one study has shown no significant difference in β-cell viability in PEG scaffolds with 50 μM to 5 mM concentrations of an immobilized laminin-mimetic peptide. However, these and many other studies do not quantify or account for differences in mechanical properties when evaluating the effect of peptides in similar PEG-peptide systems.[90,161,174–178]

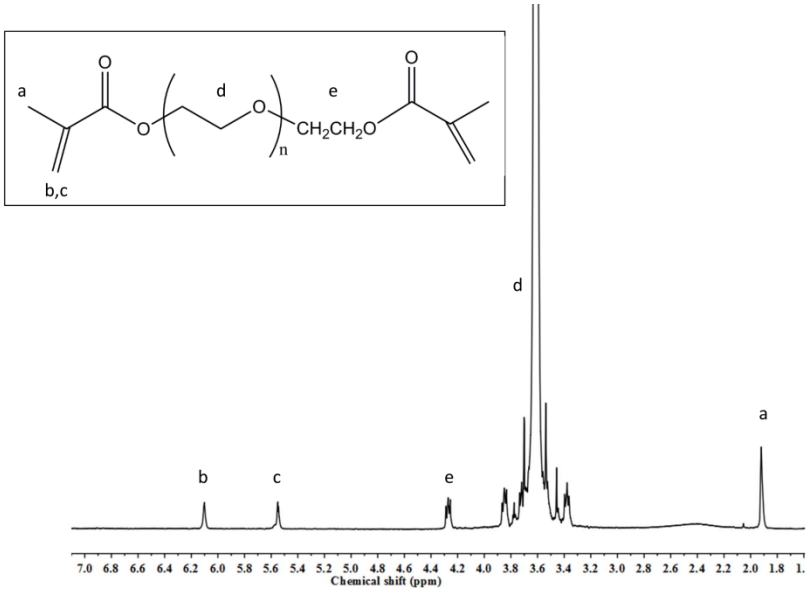

Figure 4.6: ^{1}H NMR of PEGDM10K product.

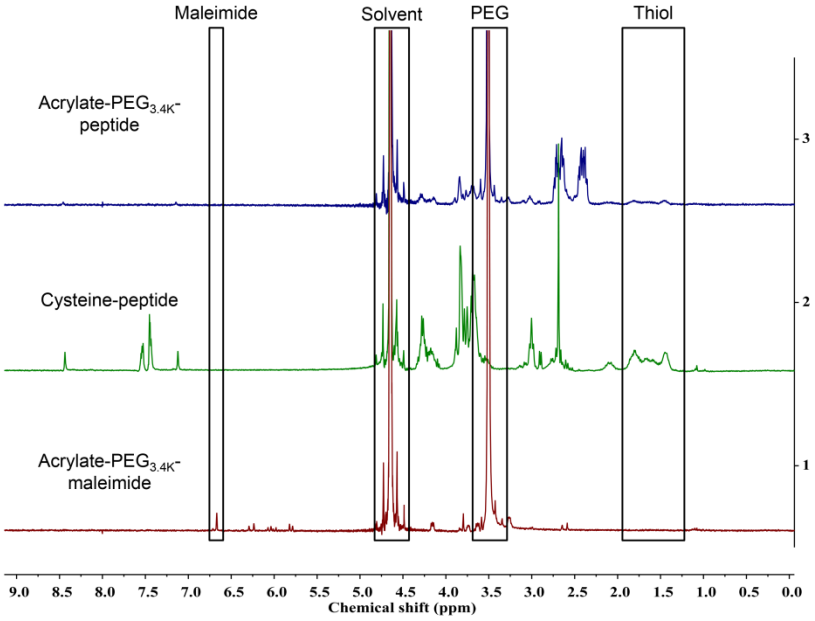

Figure 4.7: ^{1}H NMR of acryl-PEG-maleimide, cysteine peptide, and acryl-PEG-peptide product.

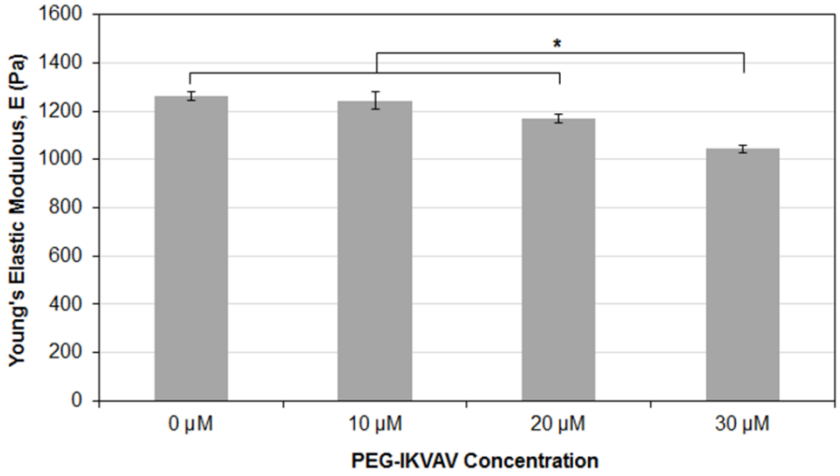

Figure 4.8: Young's elastic modulus of 10 wt % $PEGDM_{10K}$ hydrogels with various $PEG_{3.4K}$-IKVAV concentrations. Data are shown as mean ± SEM from $n \geq 3$ independent experiments (* $p < 0.05$).

4.4.4 MIN6 3D entrapment

The proliferation and insulin secretion of entrapped MIN6 cells was evaluated at d4 and d7 post-encapsulation. Proliferation results (Figure 4.9 A) show a statistically significant increase in proliferation at d4 and d7 in 20 µM acrylate-$PEG_{3.4K}$-IKVAV hydrogels compared to non-functionalized hydrogels, where proliferation is normalized to cell number immediately after encapsulation. These results are consistent with our surfaces results in 2D, showing that the presentation of the IKVAV peptide supports increased MIN6 proliferation over the blank surfaces on both d4 and d7. Insulin secretion results (Figure 4.9 B) show no statistically significant differences between MIN6 cells entrapped

in non-functionalized and IKVAV-functionalized hydrogels at d4, but by d7 the increase in insulin secretion is significant.

Results in the literature vary regarding the effect of peptides on proliferation and insulin secretion of β-cells and islets. For example, interaction with RGD and PDSGR, laminin derived recognition sequences, promoted islet viability and glucose induced insulin secretion, whereas IKVAV or DGEA (a collagen I sequence) had no effect on alginate-encapsulated human islets at days 5 and 7.[179] Mouse pancreatic islets adhered better to silk foams modified with RGD, IKVAV or YIGSR, a laminin-derived motif, compared to control wells without matrices on days 2 and 5. At day 2, islets adhered to RGD and YIGSR foam released significantly more insulin per islet compared to control islets that were free floating, but at day 5 adhered islets released the same amount of insulin per islet as did the control islets verifying that adherence to silk matrices allows maintained function. In addition, significantly less necrotic bodies were found in islets that were adhered to silk foams with no peptides or with RGD or IKVAV compared to free floating islets.[180] Survival of encapsulated MIN6 cells in PEG hydrogels diminished within one week in the absence of cell-cell and cell-matrix contacts, however, in PEG hydrogel functionalized with the laminin sequences IKLLI and IKVAV, the encapsulated β-cells maintained viability, and showed reduced apoptosis and increased insulin secretion. Interactions with other laminin sequences LRE, PDSGR, RGD, and YIGSR contributed to improved viability, but insulin release from these samples was not statistically greater

than that from controls.[161] It is important to note several significant differences between the current system and other studies that encapsulated β-cells in PEG hydrogels. Our study uses a significantly higher cell seeding density ($2x10^7$ cell/mL) compared to many other works in order to improve β-cell viability long term.[161,181] This high cell seeding concentration has been shown to maintain viable β-cells in non-functionalized PEG scaffolds for more than 10 days.[182] And yet, despite the high cell density used in our study, the presence of the IKVAV peptide in the PEG hydrogels improved cell viability and insulin secretion of the entrapped MIN6 cells. Additionally, by limiting the concentration of acrylated peptide incorporated to match the modulus of our non-functionalized control, we are able to deconvolute the effects of the peptides from the effects of hydrogel modulus where other studies have not done so.

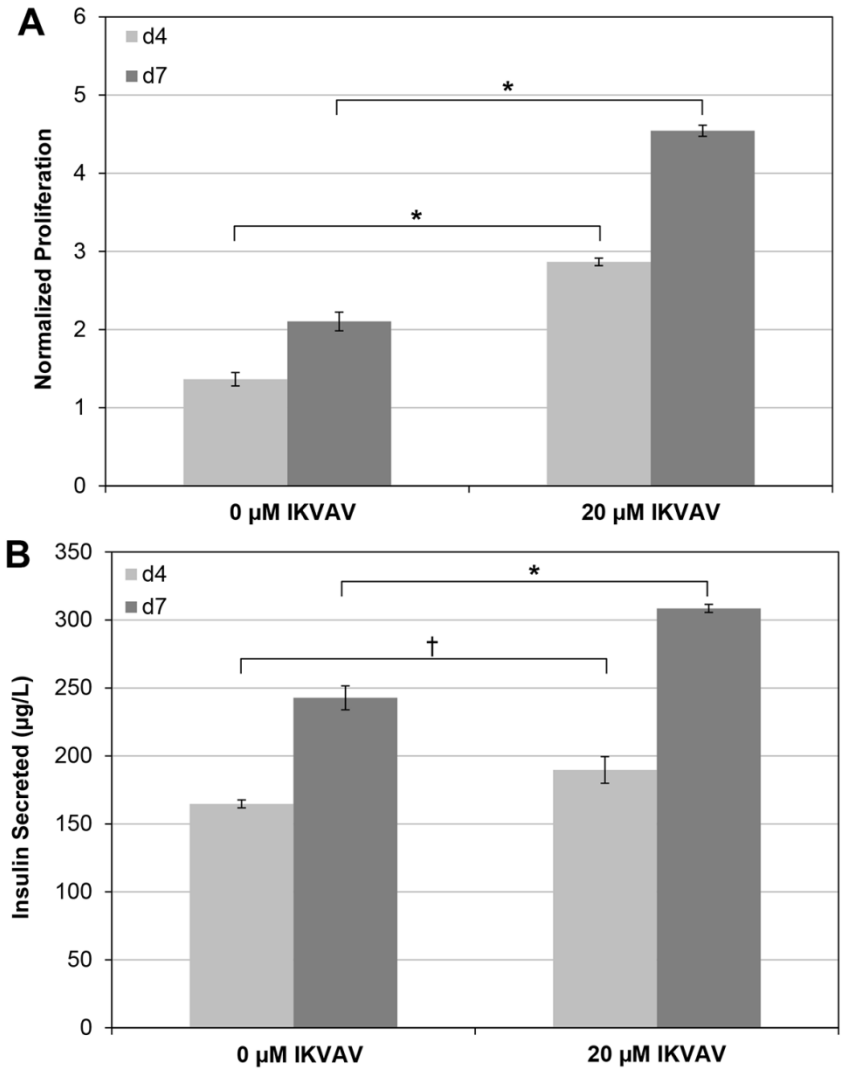

Figure 4.9: (A) Normalized proliferation of MIN6 cells encapsulated in 10 wt % PEGDM10K hydrogels at d4. Data are shown as mean ± SEM from *n*=3 independent experiments performed in quadruplicate and are normalized to gels immediately after encapsulation (t=0), * $p < 0.05$. (B) Insulin secreted from MIN6 cells encapsulated in 10 wt % PEGDM10K hydrogels at d4. Data are reported as mean ± SEM from *n*=3 independent experiments performed in triplicate.

4.5 Conclusions

Covalently immobilized peptide mimetics of ECM proteins fibronectin and laminin and growth factor ligands bFGF and GLP-1were evaluated as 2D surfaces for β-cell culture. While no synergistic effects were observed in any of the combinations of peptide mimetics, the presence of any of the four peptides studied supported an increase in proliferation and insulin secretion in MIN6 cells. Furthermore, the presence of peptides on surfaces induced a more 3D morphology or the formation of pseudoislets. The presence of the IKVAV peptide in 3D $PEGDM_{10K}$ hydrogels resulted in an increase in MIN6 proliferation and insulin secretion, consistent with 2D results. These well-defined peptide-functionalized surfaces and hydrogels can be used to probe the effects of other types of bioactive signals, including the potentially critical cell-cell signaling molecules, to obtain a better understanding of β-cell function and subsequently progress the design of scaffolds for pancreatic tissue engineering.

Chapter 5 Concluding remarks

Tissue engineering aims to regenerate functional tissues and complex organs to improve disease therapy and treatment. The major components required are viable cells and scaffolds which provide the appropriate biochemical and biophysical signals. The work in this thesis focused on the design of peptide-functionalized biomimetic scaffolds which could support three-dimensional cell culture.

Fibronectin-mimetic PR_g peptide-amphiphile hydrogels support cell adhesion, proliferation, and ECM deposition as two-dimensional surfaces. However, gelation conditions were not physiologically compatible, preventing the important translation into three dimensions. The work in Chapter 2 details the development of the E2 diluent peptide-amphiphile designed to screen the charges of the PR_g peptide-amphiphile, to increase the kinetics of gelation, and allow for assembly in physiologically relevant solutions. Fibroblasts encapsulated in PR_g/E2 hydrogels survived encapsulation, proliferated, and were well distributed throughout the hydrogel. The modulus of the PR_g/E2 hydrogels without entrapped cells was 429 Pa and 809 Pa for the 0.5 wt % and 1.0 wt % gels respectively. PR_g/E2 hydrogels with entrapped cells had significantly lower modulus than gels without cells, likely due to the disruption of the physical interactions between the nanofibers. Both weight percent formulations supported fibroblast proliferation and ECM deposition. The softer 0.5 wt % hydrogels supported

significantly greater fibroblast proliferation compared to the 1.0 wt % gels; however, the 1.0 wt % gels promoted greater increase in mRNA expression and the production of fibronectin and type IV collagen. This work not only translated out PR_g peptide-amphiphile from 2D to 3D, but also revealed an unexpected parameter for tuning hydrogel scaffolds and the cellular response.

The work presented in Chapter 3 was an effort to introduce additional bioactive peptide signal to our 3D peptide-amphiphile hydrogels. The charge of the bioactive peptide sequence had and non-trivial effect on the modulus of the peptide-amphiphile hydrogels. Our inability to decouple bioactive sequence and hydrogel modulus would have made it impossible to deconvolute the effects of the peptides and the effects of the gel modulus. This led to the investigation of the simplified, two-dimensional study discussed in Chapter 4.

Covalently immobilized peptide mimetics of ECM proteins fibronectin and laminin and growth factor ligands bFGF and GLP-1were evaluated as 2D surfaces for β-cell culture. The presence of any of these four peptides supported an increase in proliferation and insulin secretion in MIN6 cells, however no synergistic effects were observed from any of the peptide combinations. Furthermore, the presence of peptides on surfaces induced a more 3D morphology or the formation of pseudoislets. In 3D $PEGDM_{10K}$ hydrogels, the presence of the IKVAV peptide resulted in an increase in MIN6 proliferation and insulin secretion, between IKVAV-functionalized and non-functionalized gels, consistent with

2D results. These well-defined peptide-functionalized surfaces and hydrogels can be used to probe the effects of other types of bioactive signals, including the potentially critical cell-cell signaling molecules, to obtain a better understanding of β-cell function and subsequently progress the design of scaffolds for pancreatic tissue engineering.

References

(1) Lutolf, M. P. Integration Column : Artificial ECM : Expanding the Cell Biology Toolbox in 3D. *Integr. Biol.* **2009**, *1*, 235–241.

(2) Lodish, H.; Berk, A.; Kaiser, C. A.; Krieger, M.; Scott, M. P.; Bretscher, A.; Ploegh, H.; Matsudaira, P. *Molecular Cell Biology*; 6th ed.; W. H. Freeman and Company: New York, 2008.

(3) Petersen, T. E.; Thgersen, H. C.; Skorstengaard, K.; Vibe-pedersen, K.; Sahl, P.; Sottrup-jensen, L.; Magnusson, S. Partial Primary Structure of Bovine Plasma Fibronectin : Three Types of Internal Homology. *Proc. Natl. Acad. Sci. U. S. A.* **1983**, *80*, 137–141.

(4) Leahy, D. J.; Hendrickson, W. A.; Aukhil, I.; Erickson, H. P. Structure of a Fibronectin Type III Domain from Tenascin Phased by MAD Analysis of the Selenomethionyl Protein. *Science* **1992**, *258*, 987–991.

(5) Ruoslahti, E. RGD and Other Recognition Sequences for Integrins. *Annu. Rev. Cell Dev. Biol.* **1996**, *12*, 697–715.

(6) Samuel, J. L.; Farhadian, F.; Marotte, F.; Robert, V.; Rappaport, L. Expression of Fibronectin during Rat Fetal and Postnatal Development: An in Situ Hybridisation and Immunohis Tochemical Study. *Cardiovasc. Res.* **1994**, *28*, 1653–1661.

(7) Achyuta, A. K. H.; Unger, K.; Murthy, S. K. Synergistic Effect of Immobilized Laminin and Nerve Growth Factor on PC12 Neurite Outgrowth. *Biotechnol. Prog.* **2009**, *25*, 227–234.

(8) Grant, D. S.; Tashiro, K.-I.; Segui-Real, B.; Yamada, Y.; Martin, G. R.; Kleinman, H. K. Two Different Laminin Domains Mediate the Differentiation of Human Endothelial Cells into Capillary-like Structures in Vitro. *Cell* **1989**, *58*, 933–943.

(9) Discher, D. E.; Janmey, P. A.; Wang, Y.-L. Tissue Cells Feel and Respond to the Stiffness of Their Substrate. *Science* **2005**, *310*, 1139–1143.

(10) Niece, K. L.; Hartgerink, J. D.; Donners, J. J. J. M.; Stupp, S. I. Self-Assembly Combining Two Bioactive Peptide-Amphiphile Molecules into Nanofibers by Electrostatic Attraction. *J. Am. Chem. Soc.* **2003**, *125*, 7146–7147.

(11) Chiu, L. L. Y.; Radisic, M. Scaffolds with Covalently Immobilized VEGF and

Angiopoietin-1 for Vascularization of Engineered Tissues. *Biomaterials* **2010**, *31*, 226–241.

(12) Connelly, J. T.; Petrie, T. A.; García, A. J.; Levenston, M. E. Fibronectin- and Collagen-Mimetic Ligands Regulate Bone Marrow Stromal Cell Chondrogenesis in Three-Dimensional Hydrogels. *Eur. Cell. Mater.* **2011**, *22*, 168–176.

(13) Kumada, Y.; Hammond, N. A.; Zhang, S. G. Functionalized Scaffolds of Shorter Self-Assembling Peptides Containing MMP-2 Cleavable Motif Promote Fibroblast Proliferation and Significantly Accelerate 3-D Cell Migration Independent of Scaffold Stiffness. *Soft Matter* **2010**, *6*, 5073–5079.

(14) Silva, G. A.; Czeisler, C.; Niece, K. L.; Beniash, E.; Harrington, D. A.; Kessler, J. A.; Stupp, S. I. Selective Differentiation of Neural Progenitor Cells by High-Epitope Density Nanofibers. *Science* **2004**, *303*, 1352–1355.

(15) Genove, E.; Schmitmeier, S.; Sala, A.; Borros, S.; Bader, A.; Griffith, L. G.; Semino, C. E. Functionalized Self-Assembling Peptide Hydrogel Enhance Maintenance of Hepatocyte Activity in Vitro. *J. Cell. Mol. Med.* **2009**, *13*, 3387–3397.

(16) Hennessy, K. M.; Pollot, B. E.; Clem, W. C.; Phipps, M. C.; Sawyer, A. a; Culpepper, B. K.; Bellis, S. L. The Effect of Collagen I Mimetic Peptides on Mesenchymal Stem Cell Adhesion and Differentiation, and on Bone Formation at Hydroxyapatite Surfaces. *Biomaterials* **2009**, *30*, 1898–1909.

(17) Ruoslahti, E.; Pierschbacher, M. D. New Perspectives in Cell Adhesion: RGD and Integrins. *Science* **1987**, *238*, 491–497.

(18) Chou, S. Y.; Cheng, C. M.; LeDuc, P. R. Composite Polymer Systems with Control of Local Substrate Elasticity and Their Effect on Cytoskeletal and Morphological Characteristics of Adherent Cells. *Biomaterials* **2009**, *30*, 3136–3142.

(19) Kidoaki, S.; Matsuda, T. Microelastic Gradient Gelatinous Gels to Induce Cellular Mechanotaxis. *J. Biotechnol.* **2008**, *133*, 225–230.

(20) Rehfeldt, F.; Engler, A. J.; Eckhardt, A.; Ahmed, F.; Discher, D. E. Cell Responses to the Mechanochemical Microenvironment-Implications for Regenerative Medicine and Drug Delivery. *Adv. Drug Deliv. Rev.* **2007**, *59*, 1329–1339.

(21) Gray, D. S.; Tien, J.; Chen, C. S. Repositioning of Cells by Mechanotaxis on

Surfaces with Micropatterned Young's Modulus. *J. Biomed. Mater. Res. A* **2003**, *66*, 605–614.

(22) Lo, C.; Wang, H.; Dembo, M.; Wang, Y. Cell Movement Is Guided by the Rigidity of the Substrate. *Biophys. J.* **2000**, *79*, 144–152.

(23) Engler, A. J.; Sen, S.; Sweeney, H. L.; Discher, D. E. Matrix Elasticity Directs Stem Cell Lineage Specification. *Cell* **2006**, *126*, 677–689.

(24) Reilly, G. C.; Engler, A. J. Intrinsic Extracellular Matrix Properties Regulate Stem Cell Differentiation. *J. Biomech.* **2010**, *43*, 55–62.

(25) Chatterjee, K.; Lin-Gibson, S.; Wallace, W. E.; Parekh, S. H.; Lee, Y. J.; Cicerone, M. T.; Young, M. F.; Simon, C. G. The Effect of 3D Hydrogel Scaffold Modulus on Osteoblast Differentiation and Mineralization Revealed by Combinatorial Screening. *Biomaterials* **2010**, *31*, 5051–5062.

(26) Goh, S. K.; Bertera, S.; Olsen, P.; Candiello, J. E.; Halfter, W.; Uechi, G.; Balasubramani, M.; Johnson, S. a.; Sicari, B. M.; Kollar, E.; et al. Perfusion-Decellularized Pancreas as a Natural 3D Scaffold for Pancreatic Tissue and Whole Organ Engineering. *Biomaterials* **2013**, *34*, 6760–6772.

(27) Fan, Q.; Xiao, C. Effects of Crosslinking Density on Structure and Properties of Interpenetrating Polymer Networks From Polyurethane and Nitroguar Gum. *Polym. Compos.* **2008**, *29*, 758–767.

(28) Weber, L. M.; Lopez, C. G.; Anseth, K. S. Effects of PEG Hydrogel Crosslinking Density on Protein Diffusion and Encapsulated Islet Survival and Function. *J. Biomed. Mater. Res. A* **2009**, *90*, 720–729.

(29) Liu, S. Q.; Ee, P. L. R.; Ke, C. Y.; Hedrick, J. L.; Yang, Y. Y. Biodegradable Poly(ethylene Glycol)-Peptide Hydrogels with Well-Defined Structure and Properties for Cell Delivery. *Biomaterials* **2009**, *30*, 1453–1461.

(30) Greenfield, M. A.; Hoffman, J. R.; de la Cruz, M. O.; Stupp, S. I. Tunable Mechanics of Peptide Nanofiber Gels. *Langmuir* **2010**, *26*, 3641–3647.

(31) Cukierman, E.; Pankov, R.; Stevens, D. R.; Yamada, K. M. Taking Cell-Matrix Adhesions to the Third Dimension. *Science* **2001**, *294*, 1708–1712.

(32) Friedl, P.; Zänker, K. S.; Bröcker, E. B. Cell Migration Strategies in 3-D Extracellular Matrix: Differences in Morphology, Cell Matrix Interactions, and

Integrin Function. *Microsc. Res. Tech.* **1998**, *43*, 369–378.

(33) Klein, C. E.; Dressel, D.; Steinmayer, T.; Mauch, C.; Krieg, T.; Bankert, R. B.; Weber, L. Integrin α2β1 Is Upregulated in Fibroblasts and Highly Aggressive Melanoma Cells in Three-Dimensional Collagen Lattices and Mediates Reorganization of Collagen I Fibrils. *J. Cell Biol.* **1991**, *115*, 1427–1436.

(34) Birgersdotter, A.; Sandberg, R.; Ernberg, I. Gene Expression Perturbation in Vitro--a Growing Case for Three-Dimensional (3D) Culture Systems. *Semin. Cancer Biol.* **2005**, *15*, 405–412.

(35) Kim, Y.; Rajagopalan, P. 3D Hepatic Cultures Simultaneously Maintain Primary Hepatocyte and Liver Sinusoidal Endothelial Cell Phenotypes. *PLoS One* **2010**, *5*, e15456.

(36) Kudryavtseva, E. I.; Engelhardt, N. V. Requirement of 3D Extracellular Network for Maintenance of Mature Hepatocyte Morphology and Suppression of Alpha-Fetoprotein Synthesis in Vitro. *Immunol. Lett.* **2003**, *90*, 25–31.

(37) Tsang, V. L.; Chen, A. A.; Cho, L. M.; Jadin, K. D.; Sah, R. L.; DeLong, S. A.; West, J. L.; Bhatia, S. N. Fabrication of 3D Hepatic Tissues by Additive Photopatterning of Cellular Hydrogels. *Faseb J.* **2007**, *21*, 790–801.

(38) Sun, T.; Jackson, S.; Haycock, J. W.; MacNeil, S. Culture of Skin Cells in 3D rather than 2D Improves Their Ability to Survive Exposure to Cytotoxic Agents. *J. Biotechnol.* **2006**, *122*, 372–381.

(39) Gore, T.; Dori, Y.; Talmon, Y.; Tirrell, M.; Bianco-peled, H. Self-Assembly of Model Collagen Peptide Amphiphiles. *Langmuir* **2001**, *17*, 5352–5360.

(40) Hentschel, J.; Cate, M. G. J.; Bo, H. G. Peptide-Guided Organization of Peptide - Polymer Conjugates : Expanding the Approach from Oligo- to Polymers. *Macromolecules* **2007**, *40*, 9224–9232.

(41) Cui, H.; Webber, M. J.; Stupp, S. I. Self-Assembly of Peptide Amphiphiles From Molecules to Nanostructure to Biomaterials. *Biopolymers* **2010**, *94*, 1–18.

(42) Craig, J. A.; Rexeisen, E. L.; Mardilovich, A.; Shroff, K.; Kokkoli, E. Effect of Linker and Spacer on the Design of a Fibronectin-Mimetic Peptide Evaluated via Cell Studies and AFM Adhesion Forces. *Langmuir* **2008**, *24*, 10282–10292.

(43) Pashuck, E. T.; Cui, H.; Stupp, S. I. Tuning Supramolecular Rigidity of Peptide

Fibers through Molecular Structure. *J. Am. Chem. Soc.* **2010**, *132*, 6041–6046.

(44) Behanna, H. A.; Donners, J. J. J. M.; Gordon, A. C.; Stupp, S. I. Coassembly of Amphiphiles with Opposite Peptide Polarities into Nanofibers. *J. Am. Chem. Soc.* **2005**, *127*, 1193–1200.

(45) Mai, Y.; Eisenberg, A. Self-Assembly of Block Copolymers. *Chem. Soc. Rev.* **2012**, *41*, 5969.

(46) Isrealachvili, J. N. *Intermolecular and Surface Forces*; 3rd ed.; Elsevier, 2011.

(47) Griffith, L. G.; Naughton, G. Tissue Engineering — Current Challenges and Expanding Opportunities. *Science* **2002**, *295*, 1009–1014.

(48) Hartgerink, J. D.; Beniash, E.; Stupp, S. I. Self-Assembly and Mineralization of Peptide-Amphiphile Nanofibers. *Science* **2001**, *294*, 1684–1688.

(49) Paramonov, S. E.; Jun, H.-W.; Hartgerink, J. D. Self-Assembly of Peptide-Amphiphile Nanofibers: The Roles of Hydrogen Bonding and Amphiphilic Packing. *J. Am. Chem. Soc.* **2006**, *128*, 7291–7298.

(50) Jiang, H.; Guler, M. O.; Stupp, S. I. The Internal Structure of Self-Assembled Peptide Amphiphiles Nanofibers. *Soft Matter* **2007**, *3*, 454–462.

(51) Stendahl, J. C.; Rao, M. S.; Guler, M. O.; Stupp, S. I. Intermolecular Forces in the Self-Assembly of Peptide Amphiphile Nanofibers. *Adv. Funct. Mater.* **2006**, *16*, 499–508.

(52) Levitt, M. Conformational Preferences of Amino Acids in Globular Proteins. *Biochemistry* **1978**, *17*, 4277–4285.

(53) Rexeisen, E. L.; Fan, W.; Pangburn, T. O.; Taribagil, R. R.; Bates, F. S.; Lodge, T. P.; Tsapatsis, M.; Kokkoli, E. Self-Assembly of Fibronectin Mimetic Peptide-Amphiphile Nanofibers. *Langmuir* **2010**, *26*, 1953–1959.

(54) Mardilovich, A.; Craig, J. A.; McCammon, M. Q.; Garg, A.; Kokkoli, E. Design of a Novel Fibronectin-Mimetic Peptide-Amphiphile for Functionalized Biomaterials. *Langmuir* **2006**, *22*, 3259–3264.

(55) Garg, A.; Tisdale, A. W.; Haidari, E.; Kokkoli, E. Targeting Colon Cancer Cells Using PEGylated Liposomes Modified with a Fibronectin-Mimetic Peptide. *Int. J. Pharm.* **2009**, *366*, 201–210.

(56) Adil, M. M.; Levine, R. M.; Kokkoli, E. Increasing Cancer-Specific Gene Expression by Targeting Overexpressed α5β1 Integrin and Upregulated Transcriptional Activity of NF-κB. *Mol. Pharm.* **2014**, *11*, 849–858.

(57) Garg, A.; Kokkoli, E. pH-Sensitive PEGylated Liposomes Functionalized with a Fibronectin-Mimetic Peptide Show Enhanced Intracellular Delivery to Colon Cancer Cell. *Curr. Pharm. Biotechnol.* **2011**, *12*, 1135–1143.

(58) Demirgöz, D.; Pangburn, T. O.; Davis, K. P.; Lee, S.; Bates, F. S.; Kokkoli, E. PR_b-Targeted Delivery of Tumor Necrosis Factor-α by Polymersomes for the Treatment of Prostate Cancer. *Soft Matter* **2009**, *5*, 2011–2019.

(59) Demirgöz, D.; Garg, A.; Kokkoli, E. PR_b-Targeted PEGylated Liposomes for Prostate Cancer Therapy. *Langmuir* **2008**, *24*, 13518–13524.

(60) Pangburn, T. O.; Bates, F. S.; Kokkoli, E. Polymersomes Functionalized via "click" Chemistry with the Fibronectin Mimetic Peptides PR_b and GRGDSP for Targeted Delivery to Cells with Different Levels of α5β1 Expression. *Soft Matter* **2012**, *8*, 4449–4461.

(61) Shroff, K.; Rexeisen, E. L.; Arunagirinathan, M. A.; Kokkoli, E. Fibronectin-Mimetic Peptide-Amphiphile Nanofiber Gels Support Increased Cell Adhesion and Promote ECM Production. *Soft Matter* **2010**, *6*, 5064–5072.

(62) Beniash, E.; Hartgerink, J. D.; Storrie, H.; Stendahl, J. C.; Stupp, S. I. Self-Assembling Peptide Amphiphile Nanofiber Matrices for Cell Entrapment. *Acta Biomater.* **2005**, *1*, 387–397.

(63) Ma, Z.; Kotaki, M.; Inai, R.; Ramakrishna, S. Potential of Nanofiber Matrix as Tissue-Engineering Scaffolds. *Tissue Eng.* **2005**, *11*, 101–109.

(64) Chen, M.; Patra, P. K.; Warner, S. B.; Bhowmick, S. Role of Fiber Diameter in Adhesion and Proliferation of NIH 3T3 Fibroblast on Electrospun Polycaprolactone Scaffolds. *Tissue Eng.* **2007**, *13*, 579–587.

(65) Badami, A. S.; Kreke, M. R.; Thompson, M. S.; Riffle, J. S.; Goldstein, A. S. Effect of Fiber Diameter on Spreading, Proliferation, and Differentiation of Osteoblastic Cells on Electrospun Poly(lactic Acid) Substrates. *Biomaterials* **2006**, *27*, 596–606.

(66) Flemming, R. G.; Murphy, C. J.; Abrams, G. A.; Goodman, S. L.; Nealey, P. F. Effects of Synthetic Micro- and Nano-Structured Surfaces on Cell Behavior.

Biomaterials **1999**, *20*, 573–588.

(67) Gluck, J. M.; Delman, C.; Full, S.; Shemin, R. J.; Heydarkhan-Hagvall, S. Stem Cell Extracellular Matrix Interactions in Three- Dimensional System via Integrins. *J. Regen. Med.* **2013**, *2*, 1000107.

(68) Yokoi, H.; Kinoshita, T.; Zhang, S. Dynamic Reassembly of Peptide RADA16 Nanofiber Scaffold. *Proc. Natl. Acad. Sci. U. S. A.* **2005**, *102*, 8414–8419.

(69) Kleinman, H. K.; Martin, G. R. Matrigel: Basement Membrane Matrix with Biological Activity. *Semin. Cancer Biol.* **2005**, *15*, 378–386.

(70) Anderson, S. B.; Lin, C.-C.; Kuntzler, D. V.; Anseth, K. S. The Performance of Human Mesenchymal Stem Cells Encapsulated in Cell-Degradable Polymer-Peptide Hydrogels. *Biomaterials* **2011**, *32*, 3564–3574.

(71) Salinas, C. N.; Anseth, K. S. The Enhancement of Chondrogenic Differentiation of Human Mesenchymal Stem Cells by Enzymatically Regulated RGD Functionalities. *Biomaterials* **2008**, *29*, 2370–2377.

(72) Kokkoli, E.; Mardilovich, A.; Wedekind, A.; Rexeisen, E. L.; Garg, A.; Craig, J. A. Self-Assembly and Applications of Biomimetic and Bioactive Peptide-Amphiphiles. *Soft Matter* **2006**, *2*, 1015–1024.

(73) Galler, K. M.; Cavender, A.; Yuwono, V.; Dong, H.; Shi, S.; Schmalz, G.; Hartgerink, J. D.; D'Souza, R. N. Self-Assembling Peptide Amphiphile Nanofibers as a Scaffold for Dental Stem Cells. *Tissue Eng. Part A* **2008**, *14*, 2051–2058.

(74) Galler, K. M.; Aulisa, L.; Regan, K. R.; D'Souza, R. N.; Hartgerink, J. D. Self-Assembling Multidomain Peptide Hydrogels: Designed Susceptibility to Enzymatic Cleavage Allows Enhanced Cell Migration and Spreading. *J. Am. Chem. Soc.* **2010**, *132*, 3217–3223.

(75) Anderson, J. M.; Kushwaha, M.; Tambralli, A.; Bellis, S. L.; Camata, R. P.; Jun, H.-W. Osteogenic Differentiation of Human Mesenchymal Stem Cells Directed by Extracellular Matrix-Mimicking Ligands in a Biomimetic Self-Assembled Peptide Amphiphile Nanomatrix. *Biomacromolecules* **2009**, *10*, 2935–2944.

(76) Hosseinkhani, H.; Hosseinkhani, M.; Tian, F.; Kobayashi, H.; Tabata, Y. Osteogenic Differentiation of Mesenchymal Stem Cells in Self-Assembled Peptide-Amphiphile Nanofibers. *Biomaterials* **2006**, *27*, 4079–4086.

(77) Hosseinkhani, H.; Hosseinkhani, M.; Kobayashi, H. Proliferation and Differentiation of Mesenchymal Stem Cells Using Self-Assembled Peptide Amphiphile Nanofibers. *Biomed. Mater.* **2006**, *1*, 8–15.

(78) Tysseling-Mattiace, V. M.; Sahni, V.; Niece, K. L.; Birch, D.; Czeisler, C.; Fehlings, M. G.; Stupp, S. I.; Kessler, J. A. Self-Assembling Nanofibers Inhibit Glial Scar Formation and Promote Axon Elongation after Spinal Cord Injury. *J. Neurosci.* **2008**, *28*, 3814–3823.

(79) Sur, S.; Pashuck, E. T.; Guler, M. O.; Ito, M.; Stupp, S. I.; Launey, T. A Hybrid Nanofiber Matrix to Control the Survival and Maturation of Brain Neurons. *Biomaterials* **2012**, *33*, 545–555.

(80) Shah, R. N.; Shah, N. A.; Del Rosario Lim, M. M.; Hsieh, C.; Nuber, G.; Stupp, S. I. Supramolecular Design of Self-Assembling Nanofibers for Cartilage Regeneration. *Proc. Natl. Acad. Sci. U. S. A.* **2010**, *107*, 3293–3298.

(81) Lim, D.-J.; Antipenko, S. V; Vines, J. B.; Andukuri, A.; Hwang, P. T. J.; Hadley, N. T.; Rahman, S. M.; Corbett, J. A.; Jun, H.-W. Improved MIN6 β-Cell Function on Self-Assembled Peptide Amphiphile Nanomatrix Inscribed with Extracellular Matrix-Derived Cell Adhesive Ligands. *Macromol. Biosci.* **2013**, *13*, 1404–1412.

(82) Stendahl, J. C.; Wang, L.-J.; Chow, L. W.; Kaufman, D. B.; Stupp, S. I. Growth Factor Delivery from Self-Assembling Nanofibers to Facilitate Islet Transplantation. *Transplantation* **2008**, *86*, 478–481.

(83) Ghanaati, S.; Webber, M. J.; Unger, R. E.; Orth, C.; Hulvat, J. F.; Kiehna, S. E.; Barbeck, M.; Rasic, A.; Stupp, S. I.; Kirkpatrick, C. J. Dynamic in Vivo Biocompatibility of Angiogenic Peptide Amphiphile Nanofibers. *Biomaterials* **2009**, *30*, 6202–6212.

(84) Shroff, K.; Pearce, T. R.; Kokkoli, E. Enhanced Integrin Mediated Signaling and Cell Cycle Progression on Fibronectin Mimetic Peptide Amphiphile Monolayers. *Langmuir* **2012**, *28*, 1858–1865.

(85) Webber, M. J.; Tongers, J.; Renault, M.-A.; Roncalli, J. G.; Losordo, D. W.; Stupp, S. I. Development of Bioactive Peptide Amphiphiles for Therapeutic Cell Delivery. *Acta Biomater.* **2010**, *6*, 3–11.

(86) Storrie, H.; Guler, M. O.; Abu-Amara, S. N.; Volberg, T.; Rao, M.; Geiger, B.; Stupp, S. I. Supramolecular Crafting of Cell Adhesion. *Biomaterials* **2007**, *28*, 4608–4618.

(87) Sur, S.; Matson, J. B.; Webber, M. J.; Newcomb, C. J.; Stupp, S. I. Photodynamic Control of Bioactivity in a Nanofiber Matrix. *ACS Nano* **2012**, *6*, 10776–10785.

(88) Lei, Y.; Gojgini, S.; Lam, J.; Segura, T. The Spreading, Migration and Proliferation of Mouse Mesenchymal Stem Cells Cultured inside Hyaluronic Acid Hydrogels. *Biomaterials* **2011**, *32*, 39–47.

(89) Li, Y. J.; Chung, E. H.; Rodriguez, R. T.; Firpo, M. T.; Healy, K. E. Hydrogels as Artificial Matrices for Human Embryonic Stem Cell Self-Renewal. *J. Biomed. Mater. Res. A* **2006**, *79*, 1–5.

(90) Burdick, J. A.; Anseth, K. S. Photoencapsulation of Osteoblasts in Injectable RGD-Modified PEG Hydrogels for Bone Tissue Engineering. *Biomaterials* **2002**, *23*, 4315–4323.

(91) Jung, J. P.; Nagaraj, A. K.; Fox, E. K.; Rudra, J. S.; Devgun, J. M.; Collier, J. H. Co-Assembling Peptides as Defined Matrices for Endothelial Cells. *Biomaterials* **2009**, *30*, 2400–2410.

(92) Kamgoué, A.; Ohayon, J.; Tracqui, P. Estimation of Cell Young's Modulus of Adherent Cells Probed by Optical and Magnetic Tweezers: Influence of Cell Thickness and Bead Immersion. *J. Biomech. Eng.* **2007**, *129*, 523–530.

(93) Laurent, V. M.; Hénon, S.; Planus, E.; Fodil, R.; Balland, M.; Isabey, D.; Gallet, F. Assessment of Mechanical Properties of Adherent Living Cells by Bead Micromanipulation: Comparison of Magnetic Twisting Cytometry vs Optical Tweezers. *J. Biomech. Eng.* **2002**, *124*, 408–421.

(94) Dokukin, M. E.; Guz, N. V.; Sokolov, I. Quantitative Study of the Elastic Modulus of Loosely Attached Cells in AFM Indentation Experiments. *Biophys. J.* **2013**, *104*, 2123–2131.

(95) Li, Z.; Guo, X.; Palmer, A. F.; Das, H.; Guan, J. High-Efficiency Matrix Modulus-Induced Cardiac Differentiation of Human Mesenchymal Stem Cells inside a Thermosensitive Hydrogel. *Acta Biomater.* **2012**, *8*, 3586–3595.

(96) Almany, L.; Seliktar, D. Biosynthetic Hydrogel Scaffolds Made from Fibrinogen and Polyethylene Glycol for 3D Cell Cultures. *Biomaterials* **2005**, *26*, 2467–2477.

(97) Saha, K.; Keung, A. J.; Irwin, E. F.; Li, Y.; Little, L.; Schaffer, D. V; Healy, K. E. Substrate Modulus Directs Neural Stem Cell Behavior. *Biophys. J.* **2008**, *95*, 4426–4438.

(98) Janmey, P. A.; Miller, R. T. Mechanisms of Mechanical Signaling in Development and Disease. *J. Cell Sci.* **2011**, *124*, 9–18.

(99) Wex, C.; Frochlich, M.; Brandstadter, K.; Bruns, C.; Stoll, A. Experimental Analysis of the Mechanical Behavior of the Viscoelastic Porcine Pancreas and Preliminary Case Study on the Human Pancreas. *J. Mech. Behav. Biomed. Mater.* **2015**, *41*, 199–207.

(100) Kraning-Rush, C. M.; Carey, S. P.; Califano, J. P.; Smith, B. N.; Reinhart-King, C. A. The Role of the Cytoskeleton in Cellular Force Generation in 2D and 3D Environments. *Phys. Biol.* **2011**, *8*, 015009.

(101) Sengers, B. G.; Taylor, M.; Please, C. P.; Oreffo, R. O. C. Computational Modelling of Cell Spreading and Tissue Regeneration in Porous Scaffolds. *Biomaterials* **2007**, *28*, 1926–1940.

(102) Raeber, G. P.; Lutolf, M. P.; Hubbell, J. A. Molecularly Engineered PEG Hydrogels: A Novel Model System for Proteolytically Mediated Cell Migration. *Biophys. J.* **2005**, *89*, 1374–1388.

(103) Lutolf, M. P.; Lauer-Fields, J. L.; Schmoekel, H. G.; Metters, A. T.; Weber, F. E.; Fields, G. B.; Hubbell, J. A. Synthetic Matrix Metalloproteinase-Sensitive Hydrogels for the Conduction of Tissue Regeneration: Engineering Cell-Invasion Characteristics. *Proc. Natl. Acad. Sci. U. S. A.* **2003**, *100*, 5413–5418.

(104) Mandal, B. B.; Kundu, S. C. Cell Proliferation and Migration in Silk Fibroin 3D Scaffolds. *Biomaterials* **2009**, *30*, 2956–2965.

(105) Bott, K.; Upton, Z.; Schrobback, K.; Ehrbar, M.; Hubbell, J. A.; Lutolf, M. P.; Rizzi, S. C. The Effect of Matrix Characteristics on Fibroblast Proliferation in 3D Gels. *Biomaterials* **2010**, *31*, 8454–8464.

(106) Friedl, P.; Bröcker, E. B. The Biology of Cell Locomotion within Three-Dimensional Extracellular Matrix. *Cell. Mol. Life Sci.* **2000**, *57*, 41–64.

(107) Halter, M.; Tona, A.; Bhadriraju, K.; Plant, A. L.; Elliott, J. T. Automated Live Cell Imaging of Green Fluorescent Protein Degradation in Individual Fibroblasts. *Cytometry. A* **2007**, *71*, 827–834.

(108) Strebel, A.; Harr, T.; Bachmann, F.; Wernli, M.; Erb, P. Green Fluorescent Protein as a Novel Tool to Measure Apoptosis and Necrosis. *Cytometry* **2001**, *43*, 126–133.

(109) Steff, A.; Arguin, C.; Hugo, P. Detection of a Decrease in Green Fluorescent Protein Fluorescence for the Monitoring of Cell Death : An Assay Amenable to High-Throughput Screening Technologies. *Cytometry* **2001**, *243*, 237–243.

(110) Liao, H.; Munoz-Pinto, D.; Qu, X.; Hou, Y.; Grunlan, M. A.; Hahn, M. S. Influence of Hydrogel Mechanical Properties and Mesh Size on Vocal Fold Fibroblast Extracellular Matrix Production and Phenotype. *Acta Biomater.* **2008**, *4*, 1161–1171.

(111) Kisiday, J.; Jin, M.; Kurz, B.; Hung, H.; Semino, C.; Zhang, S.; Grodzinsky, A. J. Self-Assembling Peptide Hydrogel Fosters Chondrocyte Extracellular Matrix Production and Cell Division : *Proc. Natl. Acad. Sci. U. S. A.* **2002**, *99*, 9996–10001.

(112) Bryant, S. J.; Anseth, K. S. Hydrogel Properties Influence ECM Production by Chondrocytes Photoencapsulated in Poly (Ethylene Glycol) Hydrogels. *J. Biomed. Mater. Res.* **2001**, *59*, 63–72.

(113) Lamande, S. R.; Sigalas, E.; Pan, T. C.; Chu, M. L.; Dziadek, M.; Timpl, R.; Bateman, J. F. The Role of the Alpha 3(VI) Chain in Collagen VI Assembly. Expression of an Alpha 3(VI) Chain Lacking N-Terminal Modules N10-N7 Restores Collagen VI Assembly, Secretion, and Matrix Deposition in an Alpha 3(VI)-Deficient Cell Line. *J. Biol. Chem.* **1998**, *273*, 7423–7430.

(114) Hatamochis, A.; Mauch, C.; Chull, M.; Timplg, R.; Krieg, T. Regulation of Collagen VI Expression in Fibroblasts. *J. Biol. Chem.* **1989**, *264*, 3494–3499.

(115) Pires, V.; Pêcher, J.; Da Nascimento, S.; Maurice, P.; Bonnefoy, A.; Dassonville, A.; Amant, C.; Fauvel-Lafève, F.; Legrand, C.; Rochette, J.; et al. Type III Collagen Mimetic Peptides Designed with Anti- or pro-Aggregant Activities on Human Platelets. *Eur. J. Med. Chem.* **2007**, *42*, 694–701.

(116) Pêcher, J.; Pires, V.; Djaafri, I.; Da Nascimento, S.; Fauvel-Lafève, F.; Legrand, C.; Sonnet, P. Circular Dichroism Studies of Type III Collagen Mimetic Peptides with Anti- or pro-Aggregant Activities on Human Platelets. *Eur. J. Med. Chem.* **2009**, *44*, 2643–2650.

(117) Bhatnagar, R. S.; Qian, J. J.; Gough, C. A. The Role in Cell Binding of a β1-Bend within the Triple Helical Region in Collagen Al (I) Chain : Structural and Biological Evidence for Conformational Tautomerism on Fiber Surface The Role in Cell Binding. *J. Biomol. Struct. Dyn.* **1997**, 37–41.

(118) Staatz, W. D.; Fok, K. F.; Zutter, M. M.; Adams, S. P.; Rodriguez, B. A.; Santoro, S. A. Identification of a Tetrapeptide Recognition Sequence for the. *J. Biol. Chem.* **1991**, *266*, 7363–7367.

(119) Xiao, G.; Wang, D.; Benson, M. D.; Karsenty, G.; Franceschi, R. T. Role of the alpha2-Integrin in Osteoblast-Specific Gene Expression and Activation of the Osf2 Transcription Factor. *J. Biol. Chem.* **1998**, *273*, 32988–32994.

(120) Reyes, C. D.; García, A. J. Engineering Integrin-Specific Surfaces with a Triple-Helical Collagen-Mimetic Peptide. *J. Biomed. Mater. Res. A* **2003**, *65*, 511–523.

(121) Liu, Q.; Limthongkul, W.; Sidhu, G.; Zhang, J.; Vaccaro, A.; Shenck, R.; Hickok, N.; Shapiro, I.; Freeman, T. Covalent Attachment of P15 Peptide to Titanium Surfaces Enhances Cell Attachment , Spreading , and Osteogenic Gene Expression. *J. Orthop. Res.* **2012**, 1626–1633.

(122) King, W. J.; Jongpaiboonkit, L.; Murphy, W. L. Influence of FGF2 and PEG Hydrogel Matrix Properties on hMSC Viability and Spreading. *J. Biomed. Mater. Res. A* **2010**, *93*, 1110–1123.

(123) Cheng, T.-Y. Y.; Chen, M.-H. H.; Chang, W.-H. H.; Huang, M.-Y. Y.; Wang, T.-W. W. Neural Stem Cells Encapsulated in a Functionalized Self-Assembling Peptide Hydrogel for Brain Tissue Engineering. *Biomaterials* **2013**, *34*, 2005–2016.

(124) Lin, H.; Chen, B.; Sun, W.; Zhao, W.; Zhao, Y.; Dai, J. The Effect of Collagen-Targeting Platelet-Derived Growth Factor on Cellularization and Vascularization of Collagen Scaffolds. *Biomaterials* **2006**, *27*, 5708–5714.

(125) Zhang, H.; Dai, S.; Bi, J.; Liu, K.-K. Biomimetic Three-Dimensional Microenvironment for Controlling Stem Cell Fate. *Interface Focus* **2011**, *1*, 792–803.

(126) Baird, A.; Schubert, D.; Ling, N.; Guillemin, R. Receptor- and Heparin-Binding Domains of Basic Fibroblast Growth Factor. *Proc. Natl. Acad. Sci. U. S. A.* **1988**, *85*, 2324–2328.

(127) Lin, X.; Takahashi, K.; Campion, S. L.; Liu, Y.; Gustavsen, G. G.; Peña, L. A.; Zamora, P. O. Synthetic Peptide F2A4-K-NS Mimics Fibroblast Growth Factor-2 in Vitro and Is Angiogenic in Vivo. *Int. J. Mol. Med.* **2006**, *17*, 833–839.

(128) Aguirre, J. I.; Franz, S. E.; Altman, M. K.; Stabley, J. N.; Lin, X.; Zamora, P. O.;

Wronski, T. J. Skeletal Effects of Fibroblast Growth Factor Mimetic (F2A) in Ovariectomized Rats. *J. Muscukoskeletal Neuronal Interact.* **2009**, *9*, 38–43.

(129) Verrecchio, A.; Germann, M. W.; Schick, B. P.; Kung, B.; Twardowski, T.; San Antonio, J. D. Design of Peptides with High Affinities for Heparin and Endothelial Cell Proteoglycans. *J. Biol. Chem.* **2000**, *275*, 7701–7707.

(130) Ashikari-hada, S.; Habuchi, H.; Kariya, Y.; Itoh, N.; Reddi, A. H.; Kimata, K. Characterization of Growth Factor-Binding Structures in Heparin / Heparan Sulfate Using an Octasaccharide Library *. *J. Biol. Chem.* **2004**, *279*, 12346–12354.

(131) Mammadov, R.; Mammadov, B.; Toksoz, S.; Aydin, B.; Yagci, R.; Tekinay, A. B.; Guler, M. O. Heparin Mimetic Peptide Nanofibers Promote Angiogenesis. *Biomacromolecules* **2011**, *12*, 3508–3519.

(132) Rajangam, K.; Behanna, H. a.; Hui, M. J.; Han, X.; Hulvat, J. F.; Lomasney, J. W.; Stupp, S. I. Heparin Binding Nanostructures to Promote Growth of Blood Vessels. *Nano Lett.* **2006**, *6*, 2086–2090.

(133) Rajangam, K.; Arnold, M. S.; Rocco, M. A.; Stupp, S. I. Peptide Amphiphile Nanostructure-Heparin Interactions and Their Relationship to Bioactivity. *Biomaterials* **2008**, *29*, 3298–3305.

(134) Efrat, S. Genetically Engineered Pancreatic Beta -Cell Lines for Cell Therapy of Diabetes. *Ann. New York Acad. Sci.* **1999**, *875*, 286–293.

(135) Aoki, T.; Hui, H.; Umehara, Y.; LiCalzi, S.; Demetriou, A. A.; Rozga, J.; Perfetti, R. Intrasplenic Transplantation of Encapsulated Genetically Engineered Mouse Insulinoma Cells Reverses Streptozotocin-Induced Diabetes in Rats. *Cell Transplant.* **2005**, *14*, 411–421.

(136) Beck, J.; Angus, R.; Madsen, B.; Britt, D.; Vernon, B.; Nguyen, K. T. Islet Encapsulation: Strategies to Enhance Islet Cell Functions. *Tissue Eng.* **2007**, *13*, 589–599.

(137) Wang, R. N.; Rosenberg, L. Maintenance of Beta-Cell Function and Survival Following Islet Isolation Requires Re-Establishment of the Islet-Matrix Relationship. *J. Endocrinol.* **1999**, *163*, 181–190.

(138) Daoud, J.; Petropavlovskaia, M.; Rosenberg, L.; Tabrizian, M. The Effect of Extracellular Matrix Components on the Preservation of Human Islet Function in

Vitro. *Biomaterials* **2010**, *31*, 1676–1682.

(139) Mason, M. N.; Arnold, C. A.; Mahoney, M. J. Entrapped Collagen Type 1 Promotes Differentiation of Embryonic Pancreatic Precursor Cells into Glucose-Responsive Beta-Cells When Cultured in Three-Dimensional PEG Hydrogels. *Tissue Eng. Part A* **2009**, *15*, 3799–3808.

(140) Yuan, X.; Huang, Y.; Guo, Y.; Wang, L.; Guo, Q.; Xu, T.; Wu, D.; Zhou, P.; Zhu, S.; Wang, Y.; et al. Controlling the Blood Glucose of Type 1 Diabetes Mice by Co-Culturing MIN-6 Beta Cells on 3D Scaffold. *Pediatr. Transplant.* **2015**, *19*, 371–379.

(141) Beenken-Rothkopf, L. N.; Karfeld-Sulzer, L. S.; Davis, N. E.; Forster, R.; Barron, A. E.; Fontaine, M. J. The Incorporation of Extracellular Matrix Proteins in Protein Polymer Hydrogels to Improve Encapsulated Beta-Cell Function. *Ann. Clin. Lab. Sci.* **2013**, *43*, 111–121.

(142) Davis, N. E.; Beenken-Rothkopf, L. N.; Mirsoian, A.; Kojic, N.; Kaplan, D. L.; Barron, A. E.; Fontaine, M. J. Enhanced Function of Pancreatic Islets Co-Encapsulated with ECM Proteins and Mesenchymal Stromal Cells in a Silk Hydrogel. *Biomaterials* **2012**, *33*, 6691–6697.

(143) Hammar, E.; Parnaud, G.; Bosco, D.; Perriraz, N.; Maedler, K.; Donath, M.; Rouiller, D. G.; Halban, P. a. Extracellular Matrix Protects Pancreatic β-Cells against Apoptosis: Role of Short- and Long-Term Signaling Pathways. *Diabetes* **2004**, *53*, 2034–2041.

(144) Parnaud, G.; Hammar, E.; Rouiller, D. G.; Armanet, M.; Halban, P. A.; Bosco, D. Blockade of β1 Integrin-Laminin-5 Interaction Affects Spreading and Insulin Secretion of Rat β-Cells Attached on Extracellular Matrix. *Diabetes* **2006**, *55*, 1413–1420.

(145) Mirmalek-Sani, S.-H.; Orlando, G.; McQuilling, J. P.; Pareta, R.; Mack, D. L.; Salvatori, M.; Farney, A. C.; Stratta, R. J.; Atala, A.; Opara, E. C.; et al. Porcine Pancreas Extracellular Matrix as a Platform for Endocrine Pancreas Bioengineering. *Biomaterials* **2013**, *34*, 5488–5495.

(146) Raile, K.; Berthold, A.; Banning, U.; Horn, F.; Pfeiffer, C.; Kiess, W. IGFs, Basic FGF, and Glucose Modulate Proliferation and Apoptosis Induced by IFNγ but Not by IL-1β in Rat INS-1E β-Cells. *Horm. Metab. Res.* **2003**, *35*, 407–414.

(147) Olsson, R.; Carlsson, P. O. Better Vascular Engraftment and Function in

Pancreatic Islets Transplanted without Prior Culture. *Diabetologia* **2005**, *48*, 469–476.

(148) Kawakami, Y.; Iwata, H.; Gu, Y. J.; Miyamoto, M.; Murakami, Y.; Balamurugan, a N.; Imamura, M.; Inoue, K. Successful Subcutaneous Pancreatic Islet Transplantation Using an Angiogenic Growth Factor-Releasing Device. *Pancreas* **2001**, *23*, 375–381.

(149) Buteau, J.; Roduit, R.; Susini, S.; Prentki, M. Glucagon-like Peptide-1 Promotes DNA Synthesis, Activates Phosphatidylinositol 3-Kinase and Increases Transcription Factor Pancreatic and Duodenal Homeobox Gene 1 (PDX-1) DNA Binding Activity in Beta (INS-1)- Cells. *Diabetologia* **1999**, *42*, 856–864.

(150) Lin, C.-C.; Anseth, K. S. Glucagon-like Peptide-1 Functionalized PEG Hydrogels Promote Survival and Function of Encapsulated Pancreatic Beta-Cells. *Biomacromolecules* **2009**, *10*, 2460–2467.

(151) Kizilel, S.; Scavone, A.; Liu, X.; Nothias, J.-M.; Ostrega, D.; Witkowski, P.; Millis, M. Encapsulation of Pancreatic Islets within Nano-Thin Functional Polyethylene Glycol Coatings for Enhanced Insulin Secretion. *Tissue Eng. Part A* **2010**, *16*, 2217–2228.

(152) Vasavada, R. C.; Gonzalez-Pertusa, J. A.; Fujinaka, Y.; Fiaschi-Taesch, N.; Cozar-Castellano, I.; Garcia-Ocaña, A. Growth Factors and Beta Cell Replication. *Int. J. Biochem. Cell Biol.* **2006**, *38*, 931–950.

(153) Holmes, T. C.; Holmes, T. C. Novel Peptide-Based Biomaterial Scaffolds for Tissue Engineering. **2002**, *20*, 16–21.

(154) Hern, D. L.; Hubbell, J. a. Incorporation of Adhesion Peptides into Nonadhesive Hydrogels Useful for Tissue Resurfacing. *J. Biomed. Mater. Res.* **1998**, *39*, 266–276.

(155) Groß, A.; Hashimoto, C.; Sticht, H.; Eichler, J. Synthetic Peptides as Protein Mimics. *Front. Bioeng. Biotechnol.* **2015**, *3*.

(156) Raza, A.; Ki, C. S.; Lin, C.-C. The Influence of Matrix Properties on Growth and Morphogenesis of Human Pancreatic Ductal Epithelial Cells in 3D. *Biomaterials* **2013**, *34*, 5117–5127.

(157) Kuehn, C.; Dubiel, E. A.; Sabra, G.; Vermette, P. Culturing INS-1 Cells on CDPGYIGSR-, RGD- and Fibronectin Surfaces Improves Insulin Secretion and

Cell Proliferation. *Acta Biomater.* **2012**, *8*, 619–626.

(158) Lim, D.-J.; Antipenko, S. V.; Andukuri, A.; Corbett, J. A.; Jun, H.-W. Biological Sensitivity to Self-Assembled Nanomatrix Platforms Depends on the Phenotype of MIN6 -Cells. *Micro Nano Lett.* **2011**, *6*, 619.

(159) Su, J.; Hu, B. H.; Lowe, W. L.; Kaufman, D. B.; Messersmith, P. B. Anti-Inflammatory Peptide-Functionalized Hydrogels for Insulin-Secreting Cell Encapsulation. *Biomaterials* **2010**, *31*, 308–314.

(160) Dubiel, E. A.; Kuehn, C.; Wang, R.; Vermette, P. In Vitro Morphogenesis of PANC-1 Cells into Islet-like Aggregates Using RGD-Covered Dextran Derivative Surfaces. *Colloids Surfaces B Biointerfaces* **2012**, *89*, 117–125.

(161) Weber, L. M.; Hayda, K. N.; Haskins, K.; Anseth, K. S. The Effects of Cell-Matrix Interactions on Encapsulated β-Cell Function within Hydrogels Functionalized with Matrix-Derived Adhesive Peptides. *Biomaterials* **2007**, *28*, 3004–3011.

(162) Atchison, N. A.; Fan, W.; Papas, K. K.; Hering, B. J.; Tsapatsis, M.; Kokkoli, E. Binding of the Fibronectin-Mimetic Peptide, PR_b, to alpha5beta1 on Pig Islet Cells Increases Fibronectin Production and Facilitates Internalization of PR_b Functionalized Liposomes. *Langmuir* **2010**, *26*, 14081–14088.

(163) Scott, C. M.; Forster, C. L.; Kokkoli, E. 3D Cell Entrapment as a Function of the Weight Percent of Peptide-Amphiphile Hydrogels. *Langmuir* **2015**, *31*, 6122–6129.

(164) Tashiro, K.; Sephel, G. C.; Weeks, B.; Sasaki, M.; Martin, G. R.; Kleinman, H. K.; Yamada, Y. A Synthetic Peptide Containing the IKVAV Sequence from the A-Chain of Laminin Mediates Cell Attachment, Migration, and Neurite Outgrowth. *J. Biol. Chem.* **1989**, *264*, 16174–16182.

(165) Yamada, K. M. Adhesive Recognition Sequences. *J. Biol. Chem.* **1991**, *266*, 12809–12812.

(166) During, M. J.; Cao, L.; Zuzga, D. S.; Francis, J. S.; Fitzsimons, H. L.; Jiao, X.; Bland, R. J.; Klugmann, M.; Banks, W. A.; Drucker, D. J.; et al. Glucagon-like Peptide-1 Receptor Is Involved in Learning and Neuroprotection. *Nat. Med.* **2003**, *9*, 1173–1179.

(167) Masters, K. S. Covalent Growth Factor Immobilization Strategies for Tissue Repair and Regeneration. *Macromol. Biosci.* **2011**, *11*, 1149–1163.

(168) Ito, Y. Covalently Immobilized Biosignal Molecule Materials for Tissue Engineering. *Soft Matter* **2008**, *4*, 46–56.

(169) Atchison, N. A.; Swindlehurst, G.; Papas, K. K.; Tsapatsis, M.; Kokkoli, E. Maintenance of Ischemic β Cell Viability through Delivery of Lipids and ATP by Targeted Liposomes. *Biomater. Sci.* **2014**, *2*, 548–559.

(170) Lin-Gibson, S.; Bencherif, S.; Cooper, J. A.; Wetzel, S. J.; Antonucci, J. M.; Vogel, B. M.; Horkay, F.; Washburn, N. R. Synthesis and Characterization of PEG Dimethacrylates and Their Hydrogels. *Biomacromolecules* **2004**, *5*, 1280–1287.

(171) Rogers, G. J.; Hodgkin, M. N.; Squires, P. E. Cellular Physiology and Biochemistr Y Biochemistry E-Cadherin and Cell Adhesion : A Role in Architecture and Function in the Pancreatic Islet. *Cell. Physiol. Biochem.* **2007**, *19*, 987–994.

(172) Reers, C.; Hauge-Evans, A. C.; Morgan, N. G.; Willcox, A.; Persaud, S. J.; Jones, P. M. Downregulation of Proliferation Does Not Affect the Secretory Function of Transformed β-Cell Lines regardless of Their Anatomical Configuration. *Islets* **2011**, *3*, 80–88.

(173) Lin, C.; Anseth, K. S. Cell – Cell Communication Mimicry with Poly (Ethylene Glycol) Hydrogels for Enhancing β-Cell Function. *PNAS* **2011**, *108*, 1–6.

(174) Mann, B. K.; Schmedlen, R. H.; West, J. L. Tethered-TGF-Beta Increases Extracellular Matrix Production of Vascular Smooth Muscle Cells. *Biomaterials* **2001**, *22*, 439–444.

(175) Peyton, S. R.; Raub, C. B.; Keschrumrus, V. P.; Putnam, A. J. The Use of Poly(ethylene Glycol) Hydrogels to Investigate the Impact of ECM Chemistry and Mechanics on Smooth Muscle Cells. *Biomaterials* **2006**, *27*, 4881–4893.

(176) Kraehenbuehl, T. P.; Zammaretti, P.; Van der Vlies, A. J.; Schoenmakers, R. G.; Lutolf, M. P.; Jaconi, M. E.; Hubbell, J. A. Three-Dimensional Extracellular Matrix-Directed Cardioprogenitor Differentiation: Systematic Modulation of a Synthetic Cell-Responsive PEG-Hydrogel. *Biomaterials* **2008**, *29*, 2757–2766.

(177) Lee, H. J.; Lee, J.-S.; Chansakul, T.; Yu, C.; Elisseeff, J. H.; Yu, S. M. Collagen Mimetic Peptide-Conjugated Photopolymerizable PEG Hydrogel. *Biomaterials* **2006**, *27*, 5268–5276.

(178) Mann, B. K.; Gobin, A. S.; Tsai, A. T.; Schmedlen, R. H.; West, J. L. Smooth Muscle Cell Growth in Photopolymerized Hydrogels with Cell Adhesive and

Proteolytically Degradable Domains: Synthetic ECM Analogs for Tissue Engineering. *Biomaterials* **2001**, *22*, 3045–3051.

(179) Llacua, A.; de Haan, B. J.; Smink, S. A.; de Vos, P. Extracellular Matrix Components Supporting Human Islet Function in Alginate-Based Immunoprotective Microcapsules for Treatment of Diabetes. *J. Biomed. Mater. Res. Part A* **2016**, *104*, 1788–1796.

(180) Johansson, U.; Ria, M.; Åvall, K.; Dekki Shalaly, N.; Zaitsev, S. V.; Berggren, P.-O.; Hedhammar, M. Pancreatic Islet Survival and Engraftment Is Promoted by Culture on Functionalized Spider Silk Matrices. *PLoS One* **2015**, *10*, e0130169.

(181) Weber, L. M.; He, J.; Bradley, B.; Haskins, K.; Anseth, K. S. PEG-Based Hydrogels as an in Vitro Encapsulation Platform for Testing Controlled β-Cell Microenvironments. *Acta Biomater.* **2006**, *2*, 1–8.

(182) Lin, C. C.; Raza, A.; Shih, H. PEG Hydrogels Formed by Thiol-Ene Photo-Click Chemistry and Their Effect on the Formation and Recovery of Insulin-Secreting Cell Spheroids. *Biomaterials* **2011**, *32*, 9685–9695.